J. Fluid Mech. (1977), *vol.* 80, *part* 2, *pp.* 321–367
Printed in Great Britain

The role of shear-layer instability waves in jet exhaust noise

By C. J. MOORE

Advanced Research Laboratories, Rolls-Royce Limited,
P.O. Box 31, Derby, England

(Received 13 July 1976)

Large-scale structures in the form of instability waves are an inherent part of a shear-layer mixing process. Such structures are shown to be present in an acoustically and aerodynamically well behaved jet even at high Mach numbers. They do not directly radiate significant acoustic power in a subsonic jet, but do govern the production of the turbulent fluctuations which radiate broad-band jet noise. Over the whole subsonic Mach number range, a significant increase in jet noise can be produced by exciting the shear layer with a fluctuating pressure at the nozzle of only 0·08 % of the jet dynamic head but with the correct Strouhal number. Such excitation by internal acoustic, aerodynamic or thermal fluctuations could explain the variability of jet noise measurements between different rigs and could also be responsible for some components of 'excess' noise.

1. Introduction

The behaviour of jet mixing noise was first explained by the theory of aerodynamic noise developed by Lighthill (1952, 1954, 1961, 1963), and although modifications and extensions have been made by many authors they have not resulted in any basic change in the theory. Acoustically, the turbulent mixing region is equivalent to an array of convected quadrupole sources, but little is known of their detailed structure despite experimental work such as that of Davies, Fisher & Barratt (1963), which has been used to estimate the acoustic source term.

In practice, although the noise power of most jets follows the predicted eighth-power variation with velocity at moderate jet velocities, different jets produce different behaviour at lower velocities (Bushell 1971). In general, large-scale jets and engines tend to produce more noise than small-scale jets. Around 1970 several experiments were performed on model cold jets (e.g. by Lush 1971; Ahuja 1972) where precautions were taken to ensure a low level of internal turbulence and noise. The noise from these jets followed the eighth-power law to much lower velocities. More recent work shows that some of the extra noise can be explained by the effects of jet temperature (Fisher, Lush & Harper-Bourne 1973; Hoch *et al.* 1972), but many jets produce noise greater than the measured minimum under particular conditions. The difference is referred to as 'excess' noise and is often attributed to noise of internal origin such as combustion noise or strut noise.

According to Lighthill's theory the radiated jet mixing noise should depend on the fluctuating shear stress, and the simple dependence on jet velocity, density and nozzle area is a result of using measured data and applying the principles of dynamic

similarity. If, however, the structure of the jet is changed, one would expect the distribution of turbulent shear stress, and hence the radiated noise, to change.

One aspect of the jet structure which has received increasing attention in recent years is the large-scale structure with a long coherence length. Such structure was observed in low-speed jets by Crow & Champagne (1971), for example, and is also present in a different form in supersonic jets (Bishop, Ffowcs Williams & Smith 1971). Such structure has been most readily measured and visualized on two-dimensional shear layers (e.g. Brown & Roshko 1974) but measurements have also been made on circular jets (Lau 1971; Fuchs 1972*a*, *b*), and this structure has been identified as the rolling-up of the shear layer into concentrations of vorticity. This has been successfully demonstrated in numerical models by Grant (1974) and Acton (1976), for example.

The effects of this structure on the noise radiated by a subsonic jet is unknown, but Crow (1972) suggests that it is important and reports some experiments to support this. The effect on the radiated noise was also investigated by, for example, Arndt & George (1974), Hardin (1973) and Petersen, Kaplan & Laufer (1974), but no real evidence for radiation from subsonic jets was presented.

Although measurements of the noise and internal structure have been made on many jet rigs we know of no investigation where noise and internal flow measurements have been made on the same rig under the same conditions. It is therefore not known whether or not the quietest jets have coherent large-scale structures, or whether these structures affect the noise. It is also not known what, if any, structure exists for the various Reynolds and Mach numbers and various nozzle boundary-layer conditions.

We have built a jet rig with a large acoustically lined plenum chamber and taken precautions to reduce the internal acoustic noise and turbulence. This jet was tested in its natural state as described in §2, to determine its basic aerodynamic and acoustic characteristics, which were compared with other published data. Specially developed flash schlieren techniques were used to visualize the coherent jet structure over a range of subsonic Mach numbers. The results showed that, although the jet was acoustically and aerodynamically well behaved, it had a definite coherent structure. This started as an instability wave on the shear layer, was then amplified and finally rolled up into vortices which moved along the shear layer, entraining ambient air and providing large-scale mixing.

Section 3 describes experiments where the jet is excited internally by a very low level acoustic wave, which appears to act as a trigger for vortex formation and so produce regular structure, locked to the excitation. The behaviour of this structure is like that of a natural disturbance on the jet and is not inconsistent with the motions described by the shear-layer stability theory of Michalke (1971*a*, *b*, 1972) and Chan (1975). At higher levels of excitation the instability wave on the shear layer becomes nonlinear. Results are shown in §4 and at this stage the visual form of the structure changes. Under the same conditions the broad-band turbulence in the jet increases as does the far-field noise. These effects are described in §5 together with the behaviour of the radiated acoustic excitation signal.

The increase in broad-band noise in the far field is an interesting result and indicates to me that, since the broad-band noise tends to vary with jet velocity at a lower power than the eighth and usually represents an increase over the noise of the natural jet, it may be responsible for some components of excess noise. Some of the implications of this for aeroengine noise are discussed in §6.

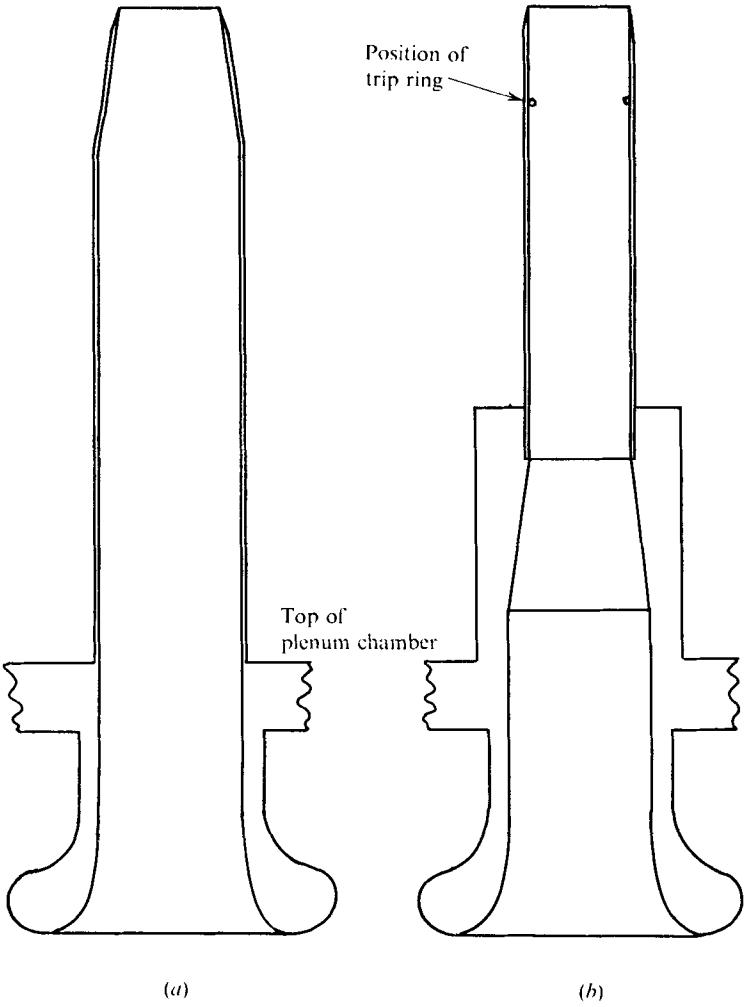

FIGURE 1. Nozzle geometry. (*a*) Conical nozzle. (*b*) Parallel nozzle, showing position of trip ring when fitted.

2. The unexcited jet

2.1. *Aerodynamic behaviour*

The jet rig used for this investigation consists of a 910 mm diameter plenum chamber which is lined with 75 mm of sound-absorbing materials. Air is supplied from a 0·5 MPa works air supply via a 150 kW heater capable of heating the air by up to 200 °C. Entry into the plenum chamber is via a 'pepper pot' arrangement consisting of a blanked pipe with many small holes in the sides.

The air leaves the plenum chamber via a small bellmouth intake which feeds a range of nozzles. All nozzles are approximately 39 mm in diameter at the lip but have different internal geometries (shown in figure 1) giving different boundary-layer thicknesses. Nozzle *A* has a parallel section $4\frac{1}{2}$ diameters long followed by a conical contraction; this produces a thin boundary layer. The mean velocity and turbulence traverses in figure 2 were obtained from hot-wire anemometer and Pitot traverses just downstream of the

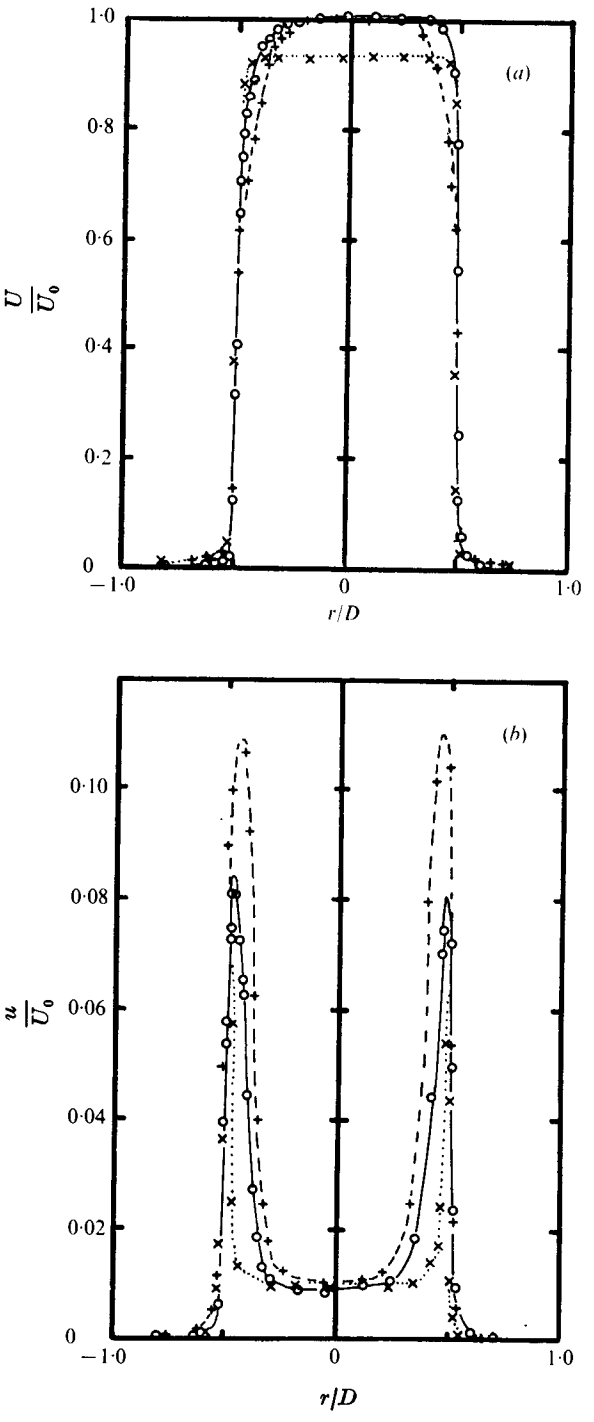

FIGURE 2. Profiles of (*a*) mean velocity and (*b*) turbulence intensity at nozzle exit. ○, parallel nozzle; – – + – –, parallel nozzle with trip; ··· × ···, conical nozzle.

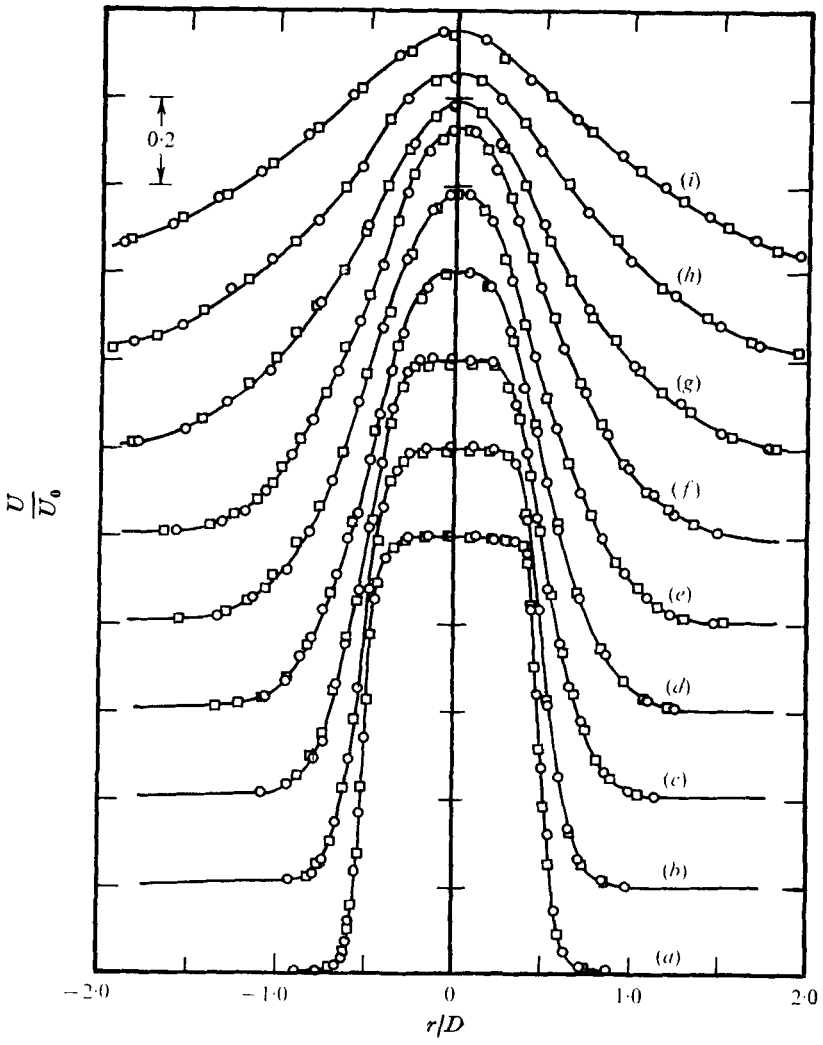

FIGURE 3. Variation of mean velocity profile with axial distance at $M = 0{\cdot}3$. ○, parallel nozzle; □, conical nozzle. (*a*) $x = D$, (*b*) $x = 2D$, (*c*) $x = 3D$, (*d*) $x = 4D$, (*e*) $x = 5D$, (*f*) $x = 6D$, (*g*) $x = 8D$, (*h*) $x = 10D$, (*i*) $x = 12D$.

nozzle lip. Nozzle *B* has a contraction followed by a parallel section $4\frac{1}{2}$ nozzle diameters long; this gives a much thicker turbulent boundary layer, which can be further thickened by the insertion of a trip ring as shown in figure 1.

The overall aerodynamic behaviour of the jets was obtained by radially traversing a hot wire at a number of axial positions up to 12 diameters downstream. The results for the mean velocity and turbulence fluctuations at a Mach number of 0·3 are shown in figures 3 and 4, where normalized results for both nozzles are plotted on the same curve. At axial distances greater than one diameter downstream, the jet velocity and turbulence profiles do not depend on the initial shear-layer thickness; the development of the profiles is independent of the initial conditions.

Figure 5 shows the axial variation of the centre-line mean velocity and turbulence intensity. The mean velocity for the conical nozzle is still increasing over the first

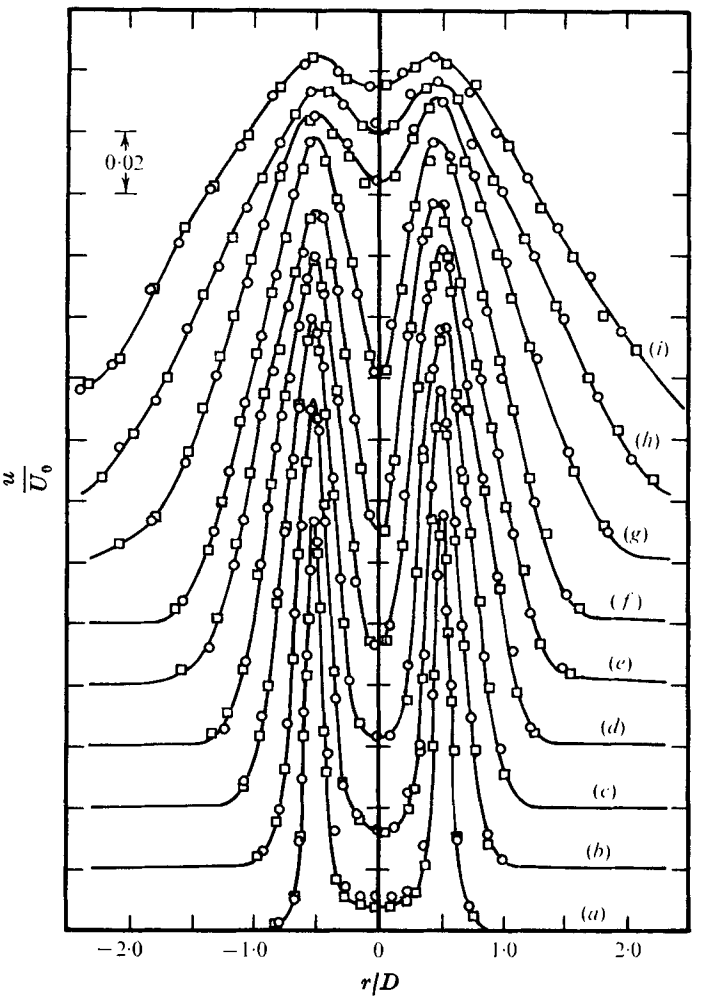

FIGURE 4. Variation of turbulence intensity profile with axial distance at $M = 0{\cdot}3$. ○, parallel nozzle; □, conical nozzle. (*a*) $x = D$, (*b*) $x = 2D$, (*c*) $x = 3D$, (*d*) $x = 4D$, (*e*) $x = 5D$, (*f*) $x = 6D$, (*g*) $x = 8D$, (*h*) $x = 10D$, (*i*) $x = 12D$.

half-diameter downstream because the nozzle acceleration has not been completed. For both jets the potential core extends to approximately 5 diameters downstream, where the mean velocity begins to fall gradually. The turbulence intensity increases gradually over the length of the potential core and then rises to a maximum of about 12½% of the mean exit velocity at a distance of approximately 8 diameters. Comparison is also made in figure 5 with the distributions measured by other experimenters. Reasonable agreement is obtained for the mean velocity but there is more variation in the turbulence intensity.

The data for axial distances of up to 6 diameters are plotted in figure 6 (*a*) against the radial distance from the nozzle lip line divided by the axial distance. This shows a very good collapse of data without a false axial zero. The mean line through these points has been redrawn in figure 6 (*b*) for comparison with other published data. The mean line from the present investigation is lower than most of the other experimental results, in

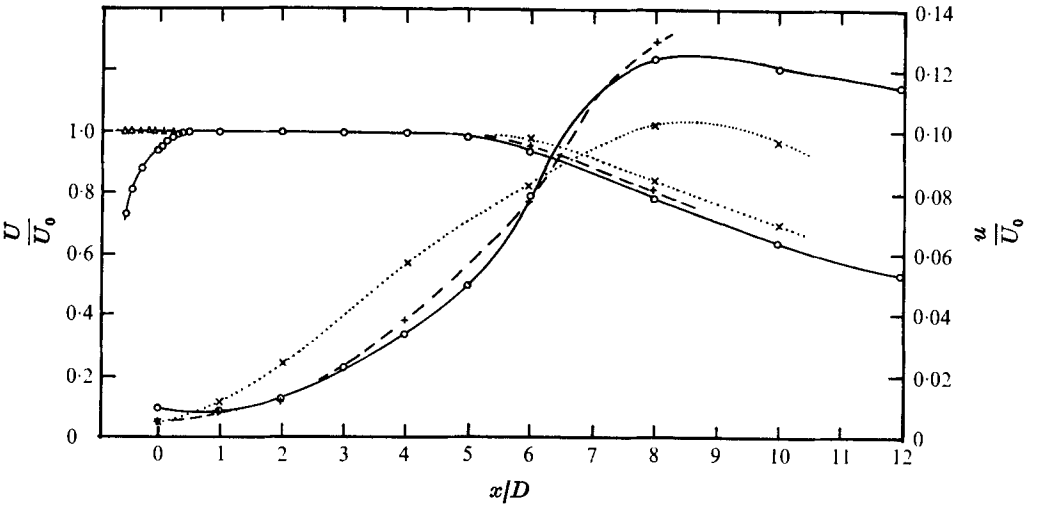

FIGURE 5. Comparison of centre-line mean velocity and turbulence with data of other experimenters. Present experiment: ○, conical nozzle; △, parallel nozzle where different. ×, Wooldridge, Wooten & Amaro (1971); +, Crow & Champagne (1971).

some cases by a considerable amount. A possible explanation for this could lie in the excitation of a pronounced instability wave on the shear layer. Crow & Champagne (1971), for example, show that, when an observable instability wave is excited, the shear layer tends to thicken. It is possible that in some of the jets enough natural excitation is present to broaden the shear layer.

2.2. *Acoustic behaviour*

The far acoustic field of the jet has been measured at a radial distance of 47 nozzle diameters in an anechoic chamber constructed around the jet using transportable panels fitted with polyurethane foam wedges 600 mm long. The chamber was tested using an impulse source, with a microphone and transient event recorder to detect reflected waves. The variation of the sound pressure level with distance from a small loudspeaker was also measured and compared with anechoic conditions. These measurements indicated that the performance of the chamber was adequate for our experiments. Far-field measurements were made using a $\frac{1}{2}$ in. diameter microphone on a continuous polar traverse which covered approximately 110° from the jet axis. The microphone signal was recorded on an FM tape recorder, with a bandwidth of 40 kHz, together with a signal indicating the position of the traversing system. The tapes were subsequently analysed by replaying them through a Bruel & Kjaer $\frac{1}{3}$ octave filter so that polar traverses in each frequency band were available. These were then processed to provide spectra or variations with jet velocity as required. Measurements were made at equal Mach number intervals from 0·3–0·9, the corresponding jet velocity being calculated from the recorded plenum-chamber temperature.

All measurements were made on both nozzles, but since they were within 0·5 dB of each other, only the results from the parallel nozzle (nozzle *B*) are presented here.

The measuring distance of 47 diameters is not really sufficient to obtain the true geometric far field of the source at low frequencies. This is because the polar traverse is

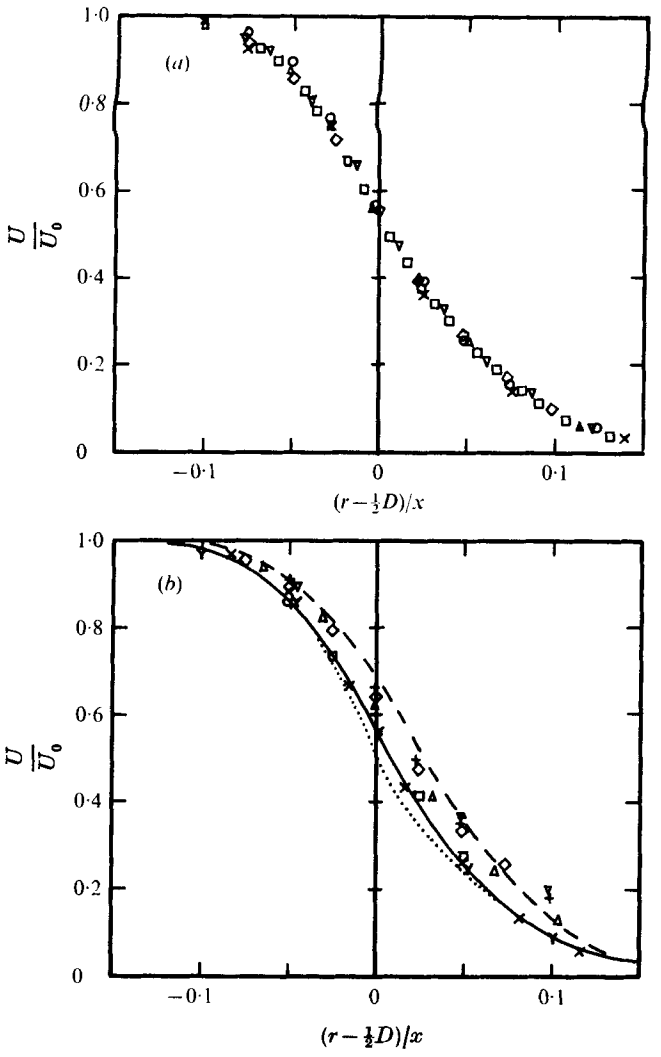

FIGURE 6. (*a*) Normalization of shear-layer profiles for potential-core region. ×, $x = D$; ○, $x = 2D$; △, $x = 3D$; ▽, $x = 4D$; ◇, $x = 5D$; □, $x = 6D$. (*b*) Comparison of normalized profiles with other experimental and theoretical data.

	x/D	D (mm)	Reference
Y	4	152	Jones & Planchon (1971)
×	2	18	Wooldridge *et al.* (1971)
◇	2	50	Bradshaw *et al.* (1964)
□	7·5	50	Bradshaw *et al.* (1964)
+	1–4	24	Ko & Davies (1971)
△	1·5–3	25·4	Davies *et al.* (1963)
▽	4	25·4	Crow & Champagne (1971)
——	1–6	39	Present work from (*a*)
.....	Theoretical		Michalke (1971*a*)
— —	Theoretical		Chan (1975)

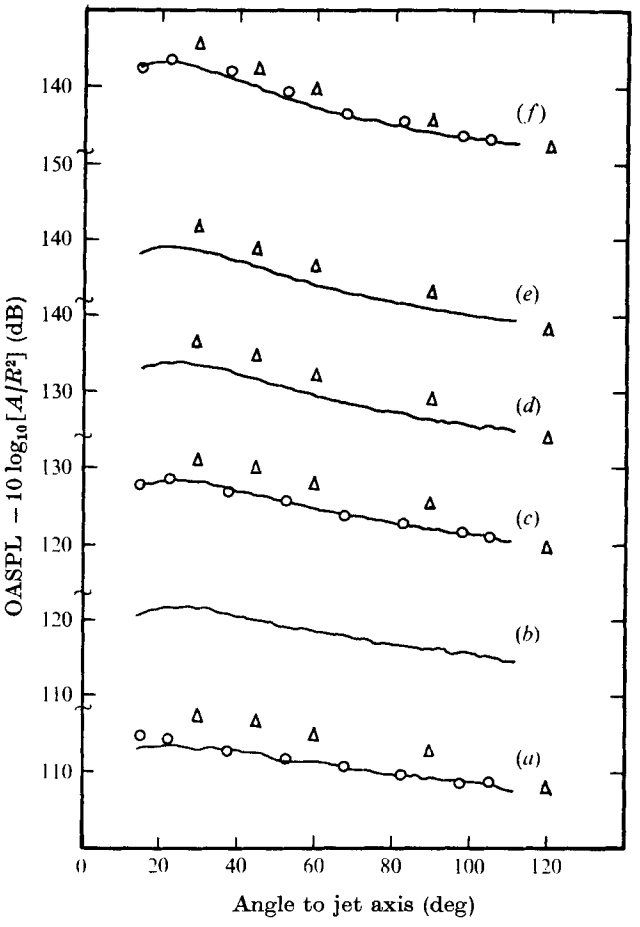

FIGURE 7. Far-field OASPL directivities of radiated jet noise. ——, present data; ○, Lush (1971); △, Ahuja (1972). Jet velocity: (*a*) $0{\cdot}39a_0$, (*b*) $0{\cdot}49a_0$, (*c*) $0{\cdot}58a_0$, (*d*) $0{\cdot}66a_0$, (*e*) $0{\cdot}75a_0$, (*f*) $0{\cdot}83a_0$.

made with respect to the nozzle exit plane whereas the low frequency sources are located far downstream. Source-location techniques such as that of Grosche (1972) have shown that the source peak at a Strouhal number of 0·1 could be approximately 15 diameters downstream. To obtain its geometric far field to an accuracy of 0·5 dB, measurements would have to be made at a radius of approximately 300 jet diameters, and, to obtain the angular directivity correct to 2°, measurements must be made at least 450 diameters from the nozzle. These distances are far greater than those normally used, the 47 diameters used here being typical of the distances used by other experimenters. Therefore no attempt to correct the measurements to give the true far field has been made.

The measured variation of OASPL (the overall sound pressure level) with angle and jet velocity is shown in figure 7. Comparison is made with other published data for quiet jets where these are available for nearly the same velocity. Corrections of up to 2 dB have been made for small differences in velocity. There is considerable scatter in the published measurements. In general the levels recorded are very much lower

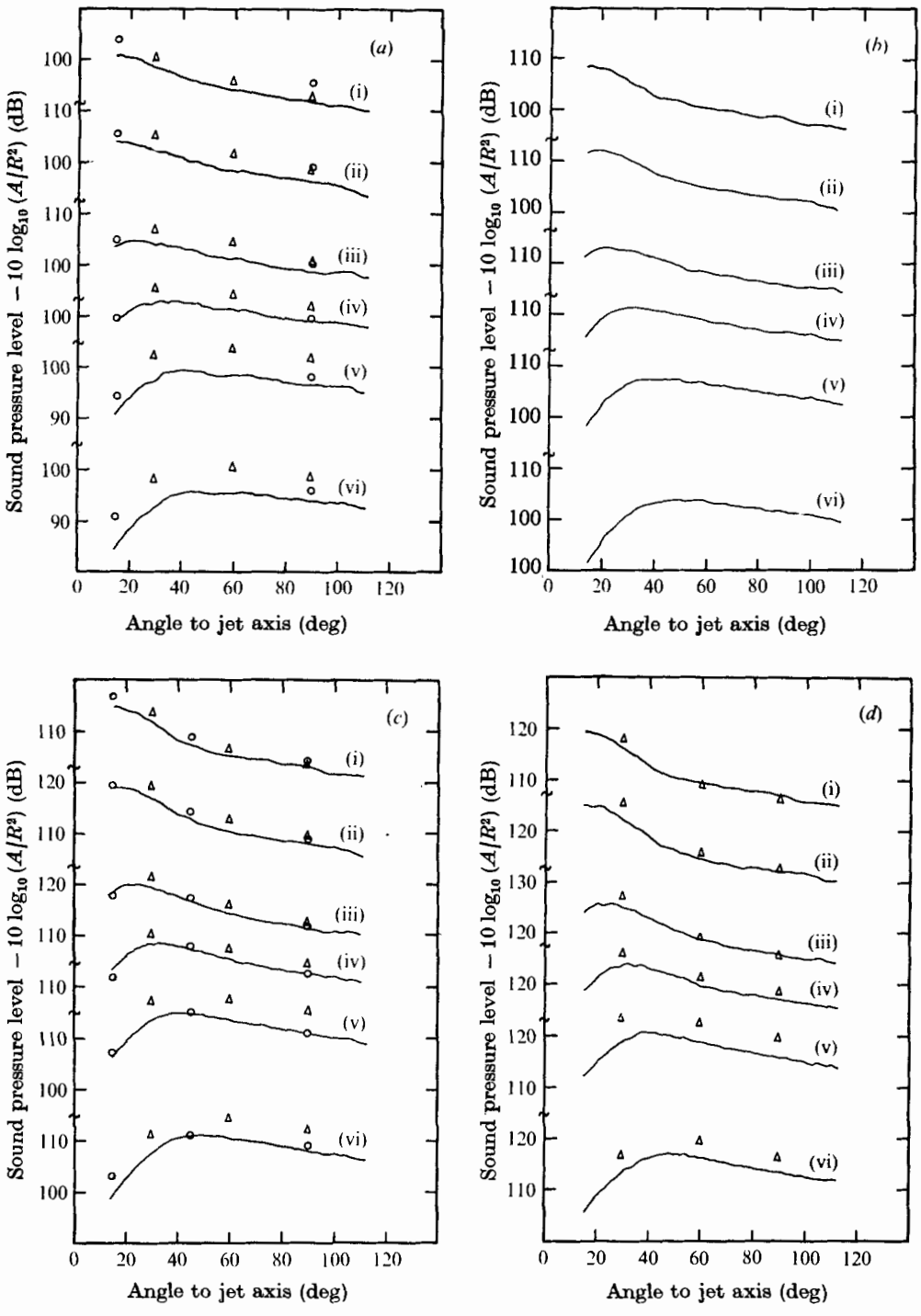

FIGURES 8 (*a–d*). For legend see facing page.

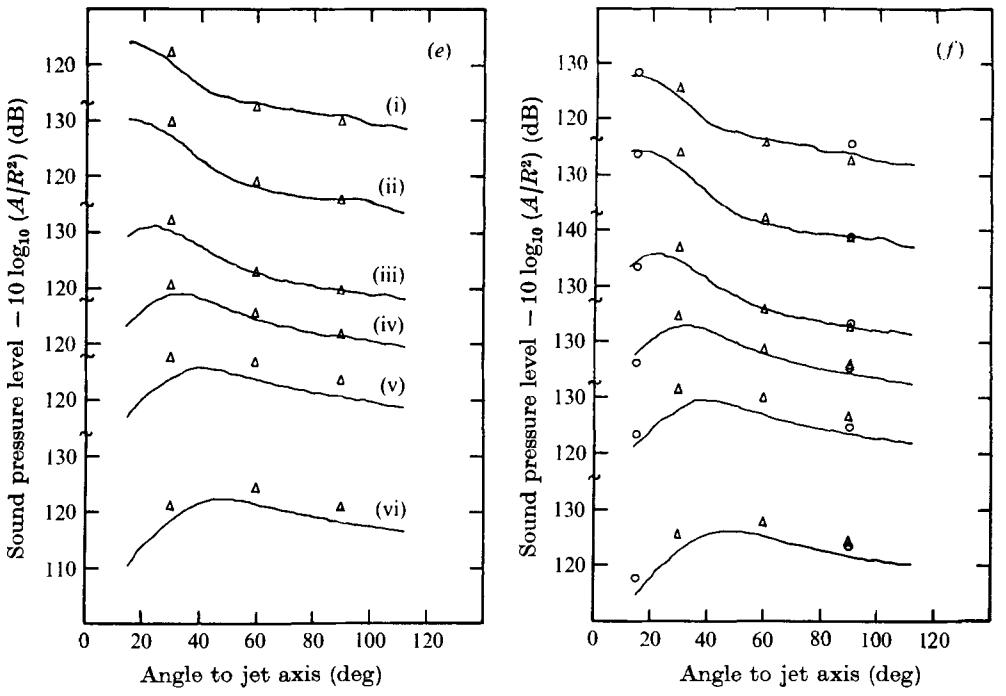

FIGURE 8. Far-field directivities of $\frac{1}{3}$ octave band filtered noise compared with other data. ○, Lush (1971); △, Ahuja (1972). Jet velocity: (*a*) $0{\cdot}39a_0$, (*b*) $0{\cdot}49a_0$, (*c*) $0{\cdot}58a_0$, (*d*) $0{\cdot}66a_0$, (*e*) $0{\cdot}75a_0$, (*f*) $0{\cdot}83a_0$. Filter centre-frequency: (i) 500 Hz, (ii) 1 kHz, (iii) 2 kHz, (iv) 4 kHz, (v) 8 kHz, (vi) 16 kHz.

than those of Ahuja (1972, 1973), whose measurements were made at approximately the same normalized distance. They are practically identical to those of Lush (1971), whose measurements were made at a distance of 120 diameters.

Figure 8 shows the $\frac{1}{3}$ octave band sound pressure level and compares this with other experimenters' results where available. Again the results agree most closely with those of Lush in most situations. Most results are lower than Ahuja's, especially at low velocities.

In general our noise levels are close to or lower than the measurements accepted as 'clean' jet noise. There is still considerable scatter between the results of the various experimenters, and this must lead to the conclusion that there are other factors, concerned with the precise construction of the rig, which affect the noise.

2.3. *Flow visualization*

Much of our basic understanding of the behaviour of flows has come from flow visualization. Such understanding not only helps in the interpretation of detailed measurements but often indicates what type of measurement should be made. One of the best recent examples is the work of Brown & Roshko (1974), who have shown very clear large-scale structures on a two-dimensional shear layer using shadowgraphs. Clear visualization of axisymmetric shear layers is more difficult to achieve but good pictures have been obtained by, for example, Bradshaw, Ferriss & Johnson (1964) and Crow & Champagne (1971), at relatively low Reynolds numbers.

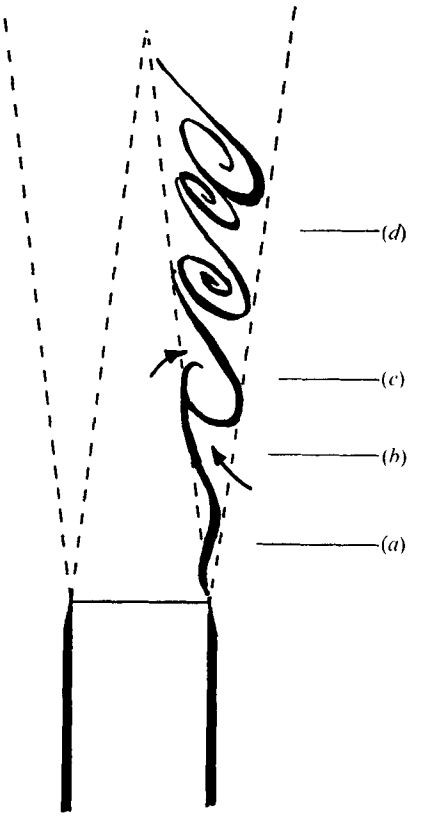

FIGURE 10. Schematic diagram of development of a jet shear layer. (*a*) Shear layer oscillates. (*b*) Air becomes entrained. (*c*) Vortices form. (*d*) Vortices form pairs and so increase axial spacing.

The flow visualization of the axisymmetric jet shown in this paper was obtained using a schlieren system with mirrors 300 mm in diameter. An initial visualization of the mixing process was obtained using a mercury arc source and a high-speed ciné camera working at approximately 14000 frames/s. Flow visualization was made easier by heating the jet air to approximately 100 °C above the ambient temperature. Films were taken over the full range of subsonic Mach numbers; examples of sections from films at Mach numbers of 0·3 and 0·9 are shown in figure 9 (plate 1). Similar characteristics are evident at the two velocities, the main difference being a slightly smaller-scale structure and narrower shear layer at the higher speed. Both examples show a dominant large-scale structure which remains coherent, allowing the disturbances to be followed on successive frames throughout the length of the jet. The general behaviour is shown diagrammatically in figure 10. The relatively thin shear layer near the nozzle is initially excited by flow disturbances from which an instability wave grows and eventually rolls up into a vortex, entraining ambient air. These vortices grow to produce an unstable array as described by Winant & Browand (1974) for example. One vortex appears to pass inside the preceding one and in so doing amalgamates with it or possibly is destroyed (Moore & Saffman 1975). This process is shown in figure 11, which follows the development of the vortex structure on one side of the shear layer according to successive frames of the high-speed ciné film. This

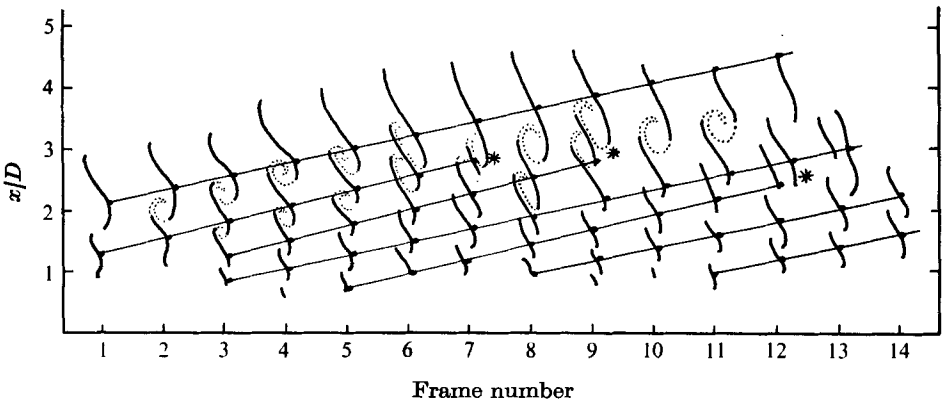

FIGURE 11. Tracings from successive frames of a high-speed ciné film showing development and eventual disappearance of vortices, marked by stars (92 μs between frames).

motion could also be considered as the growth of a larger-scale instability wave at the expense of the smaller-scale wave which was present on the narrower upstream shear layer.

We have developed a method for averaging out the random fluctuations which mask the development of the large-scale structure in the ciné films. A flash schlieren system using an argon arc source was set up and several successive flash exposures were made on one 35 mm negative. If the flashes occur randomly, then the jet is visualized as a general grey area since the large density gradients occur at random positions. If the flashes are synchronized to the large-scale structure, the large density gradients caused by ambient air being entrained in the vortices always occur at the same position, so that bright areas start to form. The development of the averaged structure as more flashes are superimposed is shown in figure 12 (plate 2). As more exposures are added, the large-scale structure becomes clearer since successive images of this structure always occur at approximately the same position. Several different methods of triggering were used and some results for 15 superimposed flashes are shown in figure 13 (plate 3). A hot-wire anemometer at various positions in the mixing region was found to be too sensitive to the high frequency turbulence and hence showed no large-scale structure. The two other methods produced a more integrated effect and hence averaged out the small-scale structure. Figure 13(*b*) shows the results obtained by passing a laser beam tangentially through the shear layer and using its deflexion to trigger the flash. Figure 13(*c*) shows the results of using a $\frac{1}{4}$ in. microphone in the jet near field. The two methods produce similar results and the microphone system was chosen as being the more convenient to use.

It is interesting to note that the large-scale structure is visible only on the side of the jet where the triggering signal is obtained although it must be present on both sides. Closer inspection of the high-speed ciné films shows that the structure is sometimes present in a symmetric mode and sometimes in an asymmetric mode. The two modes average out on the side opposite the trigger.

We have developed a method for detecting which mode is present using an equally spaced circular array of six microphones. The outputs of the microphones are added and subtracted with appropriate weighting functions in order to perform a circumferential

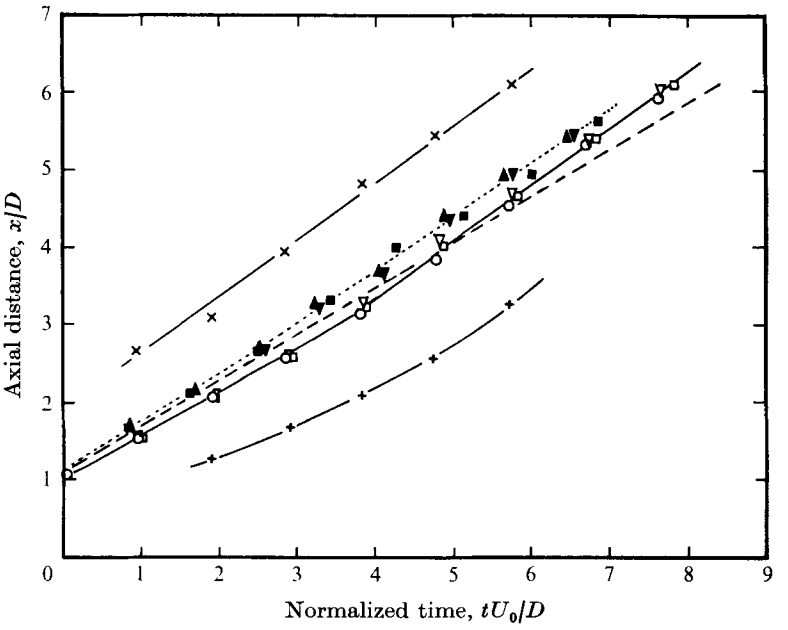

FIGURE 15. Development of large-scale structure from averaged flash schlieren photographs.

Cold	Warm		
▲	△	$U_0 = 0{\cdot}83a_0$	
▼	▽	$U_0 = 0{\cdot}66a_0$	
■	□	$U_0 = 0{\cdot}49a_0$	
	×	Disturbance preceding trigger	$U_0 = 0{\cdot}3a_0$
	○	Triggering disturbance	
	+	Disturbance following trigger	
.....	——	Average line	
	- - - -	Convection speed $= 0{\cdot}6U_0$	

Fourier analysis of the pressure pattern. The signal obtained from the zero-order mode and the part of the first-order mode in the plane perpendicular to the direction of view are then delayed and used as trigger signals for the flash system.

In figure 14 (plates 4 and 5) we show the development of the averaged axisymmetric and first-order azimuthal modes for Mach numbers of 0·3 and 0·9. The array of microphones used as a trigger is clearly visible at about one diameter downstream of the nozzle. The time increment between frames is 0·3 ms and 0·1 ms for $M = 0{\cdot}3$ and $M = 0{\cdot}9$ respectively and the final frame in each sequence is for 15 superimposed random exposures. Although the jet was heated by 100 °C for $M = 0{\cdot}3$, it was unheated for $M = 0{\cdot}9$, and this probably accounts for the change in the apparent shape of the jet. In the unheated jet, once the gases from the two streams have the same velocity they do not show density gradients, whereas in the heated jet the density gradients persist until small-scale mixing of the hot and cold streams has taken place.

Figure 14 shows not only the disturbance which was used as a trigger but also one and sometimes two before and after it. This indicates a long coherence length which probably represents a resonant response of the shear layer. Also, as was seen from the ciné films, the structure maintains its identity over an axial length of at least five jet diameters. Identical results were obtained for the three nozzle configurations,

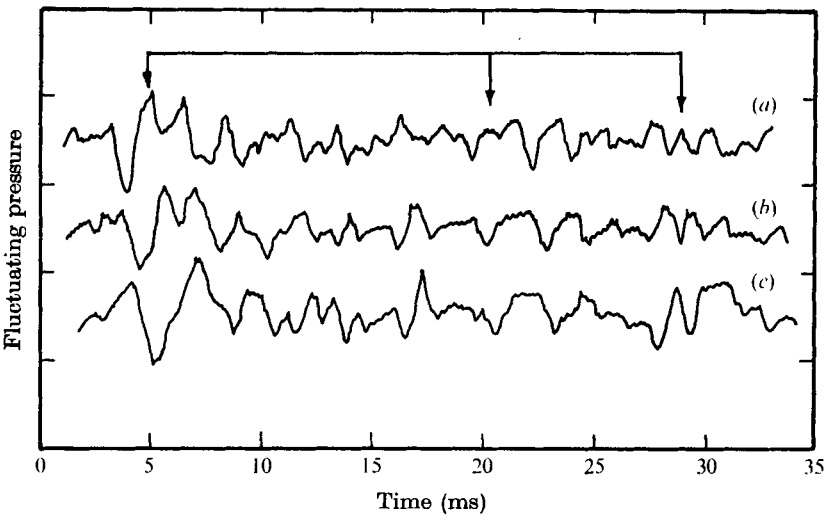

FIGURE 16. Simultaneous microphone traces at different axial positions showing disappearance of vortices. Microphones at axial distances of (*a*) 3*D*, (*b*) 4*D* and (*c*) 5*D*.

which produced boundary layers ranging from a very thin boundary layer to the thick turbulent boundary layer obtained using a trip ring. This again shows the insensitivity of the later development of the shear layer to the behaviour within the first diameter downstream. From sequences similar to those shown in figure 14 it is possible to obtain the mean convection speed of the structure. Plots of axial position against normalized time for a range of Mach numbers and for heated and unheated jets are shown in figure 15 for the plane wave mode. The higher-order azimuthal modes exhibit similar behaviour. The speed of the disturbance from which the trigger is obtained is less than 0·6 of that of the mean flow at the start and then increases to nearly 0·7 after about three diameters downstream. The disturbance on the cold jet is slightly slower than that on the warm jet, but does not change in speed with Mach number.

Also shown in figure 15 is the progress of the disturbances which precede and follow the triggering disturbance for the heated jet with Mach number 0·3. As the train of waves moves downstream, the effective wavelength increases and some of the individual disturbances must disappear as was shown from the high-speed ciné schlieren films. Since this occurs randomly it probably causes the limitations of the apparent coherence length of the disturbance. The spacing of the vortices near the end of the potential core corresponds to a Strouhal number of approximately 0·5, which is approximately the Strouhal number for peak noise radiation.

Other evidence for the disappearance of vortices can be seen in figure 16, which shows the signals from the axially spaced microphones close to the jet. The traces are, approximately, time-delayed versions of each other except at certain times when significant peaks in the wave form disappear between microphones; these times are indicated by the arrows.

In an attempt to visualize the behaviour of the shear layer close to the nozzle, some single-flash schlieren photographs were taken of this region. These were triggered from a $\frac{1}{4}$ in. diameter microphone which can be seen in the corner of figure 17 (plate 6). The total length of shear layer visible here is approximately $\frac{1}{2}D$. It can be seen that, even in

this region, there are relatively large scale-movements of the shear layer which probably provide the mechanism for mixing. Near the nozzle, the spacing is a tenth of a jet diameter or less, but owing to vortex amalgamation the spacing increases as the shear layer broadens.

3. Low-level excitation

3.1. *Basic behaviour with excitation*

The natural behaviour of the jet shear layer described in § 2 involves the development of instability waves and the subsequent rolling-up of the layer into vortices. We regard this process as the natural mechanism for the mixing between the two dissimilar streams. The folding of the two flows into each other caused by the vortices effectively increases the surface contact area and permits the effects of small-scale diffusion, which is a relatively slow process, to accumulate more quickly.

We have seen that plane waves and first-order azimuthal modes are definitely present in the unexcited jet at all subsonic velocities. It is most probable that the main source of this excitation is turbulence since the only upstream acoustic wave which could be present is a plane wave in the 0·5 Strouhal number range as shown by the duct cut-off curve in figure 18. The excitation depends not only on the amplitude of the disturbance measured at a point but also on the correlation with the fluctuations at other points. Although there is natural turbulence of intensity approximately 1 % in the nozzle plane, measurements have shown that only about 1 % of this is correlated across the nozzle plane.

An acoustic wave has been applied to the shear layer by using an acoustic horn assembly mounted within the plenum chamber. The frequency range of the excitation can automatically limit the response to plane waves over much of the velocity range as shown above, making the interpretation of measurements much simpler.

The response of the shear layer can be considered for two regimes: at low excitation levels the response is linearly related to the input, whilst at higher levels the response becomes nonlinear. In this section we shall limit discussion to the linear regime, which, in the peak response range of Strouhal numbers, limits the fluctuating pressure to less than 0·08 % of the jet dynamic head.

Figure 19 (plate 7) shows some averaged flash schlieren photographs taken for a jet with a low level of acoustic excitation at a Strouhal number of approximately 0·5 and a Mach number of 0·5. The flashes are triggered from the electrical signal fed to the horn driver. Over an axial distance equivalent to one diameter downstream, there is no synchronized structure, because the excitation is of the wrong wavelength for the instability wave to amplify. Thereafter the structure is of a similar form to the natural jet structure but the disturbances are more equally spaced and have a longer coherence length. As will be seen later, each excitation frequency is most amplified at a particular axial distance. When there is a principal frequency of excitation this will dominate even at a position where it is not maximally amplified. Thus there is not much variation in the dominant frequency with distance and the coherence length is greater.

In the region of low excitation, it might be possible to describe the behaviour of the shear layer in terms of linear stability theory. Detailed measurements have therefore been made inside the jet to determine the quantitative behaviour of the wave.

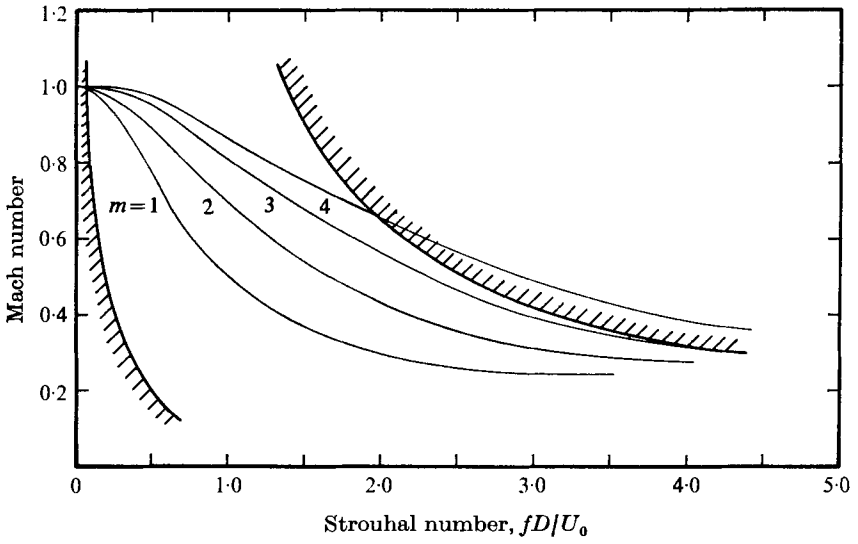

FIGURE 18. Chart showing Mach number and Strouhal number criteria for propagation of mth circumferential mode in nozzle duct. Thick line shows range of present tests.

3.2. *Measurements of internal structure*

Since the excitation of the jet is axisymmetric, most of the measurements of the jet structure have been made on the jet centre-line. The main measurements have been made with a $\frac{1}{4}$ in. microphone with a nose cone pointing into the flow. The pressure is sensed through a gauze at the side of the nose cone so that fluctuations in the static pressure are measured. Measurements have also been made using a constant-temperature hot-wire anemometer. This determines the fluctuating axial velocity at low Mach numbers, but at higher Mach numbers becomes seriously affected by pressure and temperature fluctuations. The velocity data presented have therefore been limited to Mach numbers below 0·5. Both pressure and velocity signals are filtered with a 3 Hz band-pass filter, set at the excitation frequency so that only the instability wave component of the fluctuation is measured.

Figure 20 shows the axial variation of the fluctuating pressure for a range of flow rates and for the three frequencies corresponding to the peaks of the driving system's response. These frequencies were used in most of the subsequent tests. Inside the upstream duct, axial standing waves are formed because of reflexions of the acoustic wave from the nozzle exit. The positions and separations of maxima and minima vary as the flow rate changes owing to the convection of the waves and the change in nozzle impedance. The amplitude of the pressure wave also changes, and this effect will be further investigated in §5.2.

Far outside the nozzle, with no flow, the sound pressure falls according to the inverse square law, but flow distorts this field and causes the sound pressure to reach a minimum and then rise at a rate which depends on the frequency and flow speed. Each curve reaches a maximum and then slowly decays. There are two reasons for the rise in internal fluctuating pressure: first, the pressure wave propagates along the potential core, and second, it excites the instability wave on the shear layer. When the amplification of the instability wave is small it can be of the same order as the acoustic wave, and

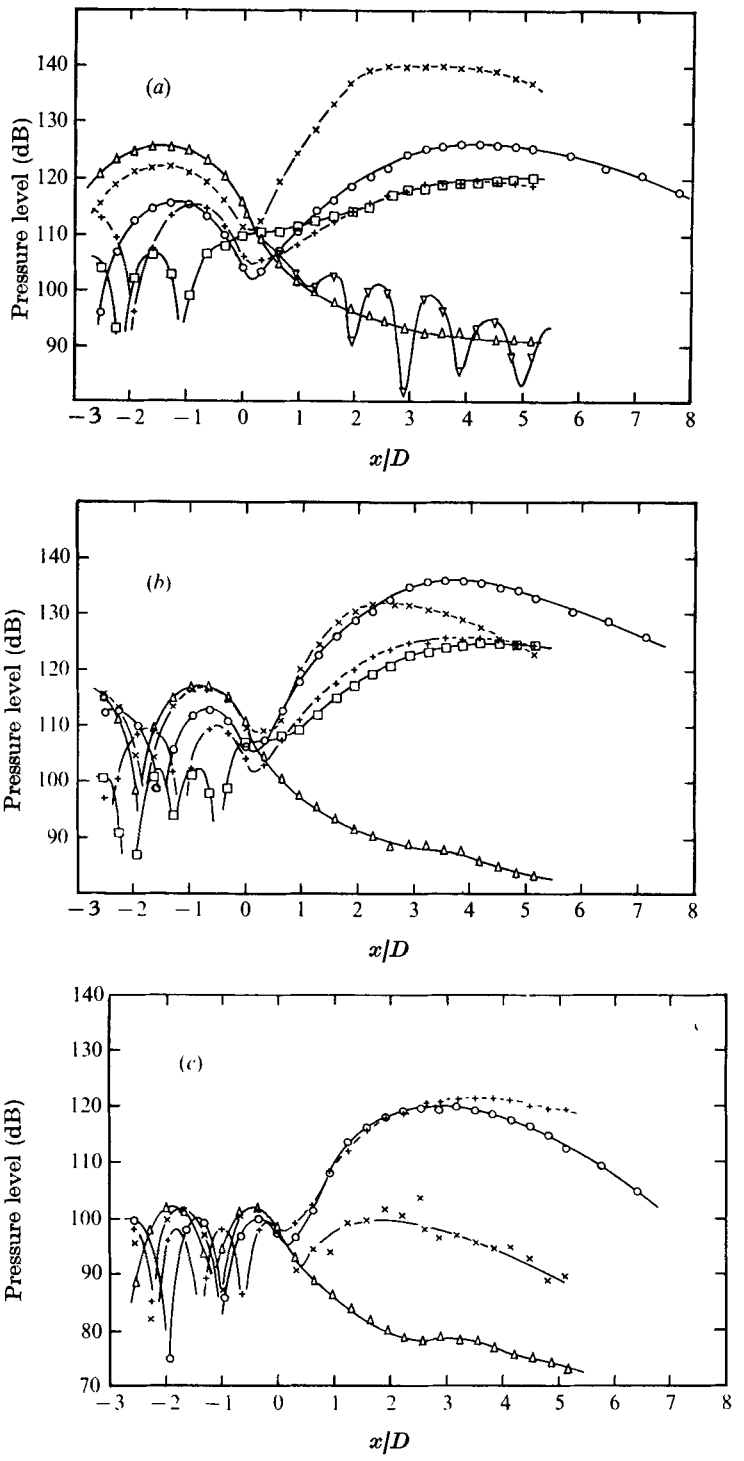

FIGURE 20. Axial variation of pressure level on jet centre-line with jet excited at (*a*) 1281 Hz, (*b*) 2050 Hz and (*c*) 3254 Hz in the linear range. Jet velocity: △, 0·0; ▽, 0·15a_0; ×, 0·3a_0; ○, 0·49a_0; +, 0·66a_0; □, 0·83a_0.

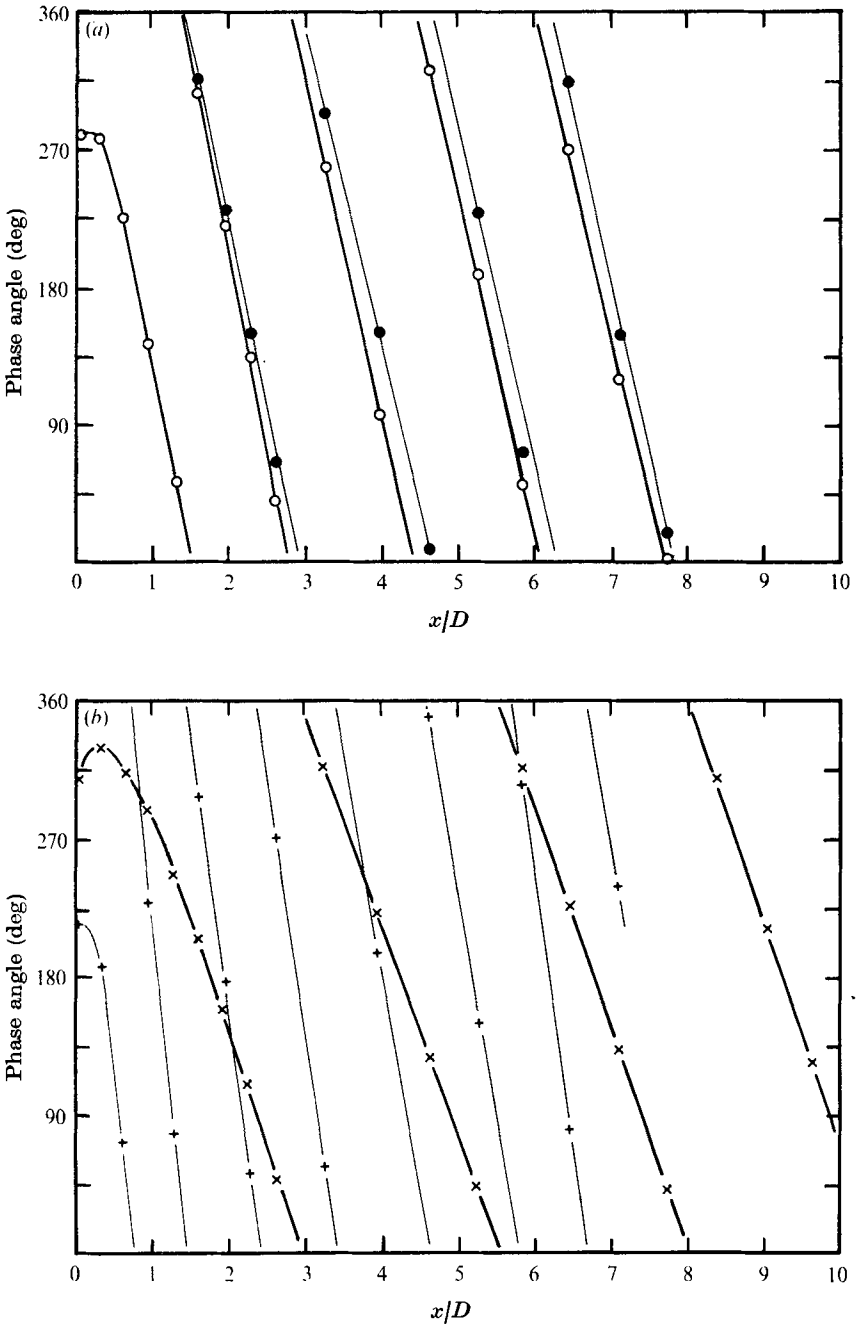

FIGURE 21. Measured phase angle of pressure signal referred to driver source along centre-line of jet at $U_0/a_0 = 0{\cdot}49$. ×, $f = 1281$ Hz; ○, $f = 2050$ Hz, low level; ●, $f = 2050$ Hz, high level; +, $f = 3254$ Hz.

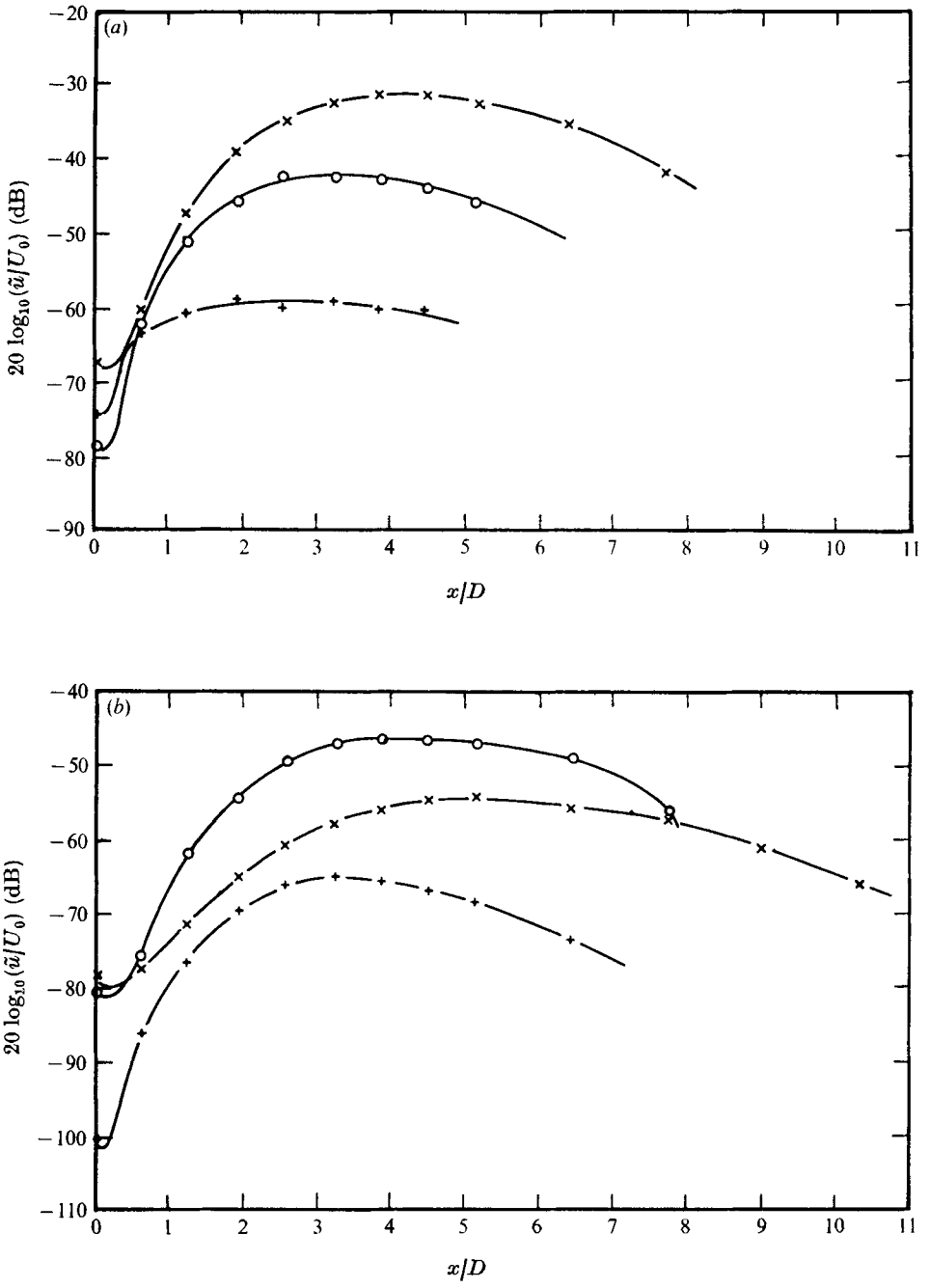

Figure 22. Variation of instability wave axial fluctuating velocity on jet axis, at jet velocities of (*a*) $0{\cdot}3a_0$ and (*b*) $0{\cdot}49a_0$. Low-level excitation at: ×, 1281 Hz; ○, 2050 Hz; +, 3254 Hz.

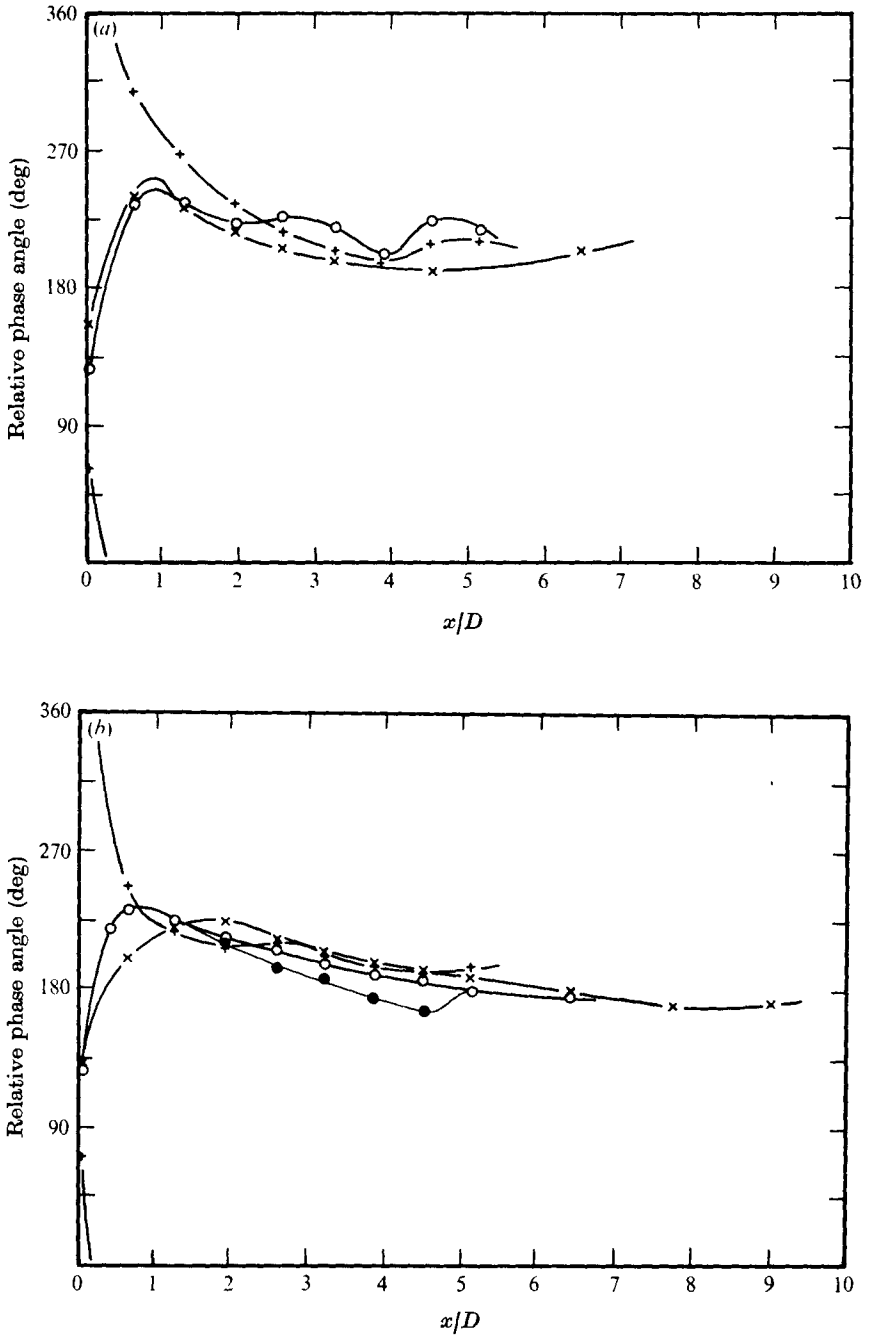

FIGURE 23. Axial variation of phase angle between velocity and pressure on jet centre-line at jet velocities of (*a*) $0{\cdot}3a_0$ and (*b*) $0{\cdot}49a_0$. Low-level excitation at: ×, 1281 Hz; ○, 2050 Hz; +, 3254 Hz. High-level excitation at: ●, 2050 Hz.

although they both have the same frequency, their speeds of propagation are different, producing interference patterns, as shown for $M = 0{\cdot}15$ in figure 20(*a*). This behaviour has previously been noted by Pfizenmaier (1973). Under most of the conditions tested, the amplitude of the pressure field of the instability wave is considerably greater than that of the acoustic wave, so that no significant interference patterns are formed and the measurements can be taken as measurements of the instability wave.

The phase angle of the pressure signal on the axis of the jet referred to the driving signal is shown in figure 21 for a Mach number of 0·5. The curve is flat or rises slightly just downstream of the nozzle, then as the instability wave amplitude begins to dominate the pressure field the phase angle starts to fall at an approximately constant rate. The slope of the curve increases with frequency and decreases as the flow velocity is increased.

The variation on the axis of the jet of the fluctuating axial velocity associated with the instability wave is shown in figure 22 for Mach numbers of 0·3 and 0·5. The shapes of the curves are similar to those of the fluctuating pressure, but the amplification rates are higher by up to 6 dB.

Figure 23 shows the variation of the phase angle between the velocity and pressure fluctuations. At the nozzle the acoustic wave still dominates. Since this is in the form of a standing wave in the duct, the phase angle is approximately 90°. As the acoustic wave passes through a pressure minimum just outside the nozzle the phase angle changes rapidly to 270°, the direction of the change depending on whether the upstream or downstream acoustic wave is of greater magnitude. This will be discussed in more detail in §5.2. Before the phase actually reaches 270°, the instability wave starts to dominate and at one diameter downstream the phase is approximately 220°–250°. Further downstream the phase gradually decreases until it is approximately 180° near the end of the region where the wave is amplified.

3.3. *Comparison with theory*

The instability wave on the shear layer grows at a rate which depends mainly on the shear-layer thickness, the frequency of excitation and the flow speed, although there is also some dependence on the Reynolds number, Mach number and temperature ratio. The behaviour will also be different for different azimuthal mode orders, but our discussion will have to be limited to the plane wave for which measurements are available. We can describe the behaviour of the pressure wave at a distance $x+x'$ by

$$p_{x+x'} = p_x \exp(-\alpha_i x') \exp[i\alpha_r (x' - C_{\mathrm{ph}} t)],$$

with a similar form for the fluctuating velocity. α_r and α_i are the real and imaginary parts of the wavenumber, C_{ph} is the phase speed of the disturbance and the applied frequency is given by $C_{\mathrm{ph}}\alpha_r$. The value of the wavenumber is correct only for a limited axial distance x', since it depends critically on the shear-layer thickness, which varies with axial distance.

The integrated effect of the amplification rate gives the total pressure wave amplitude at each axial station. The maximum amplification appears to be mainly a function of the Strouhal number, as shown in figure 24. The maximum amplification available is 30 dB for the pressure wave and 36 dB for the velocity wave, which are both greater

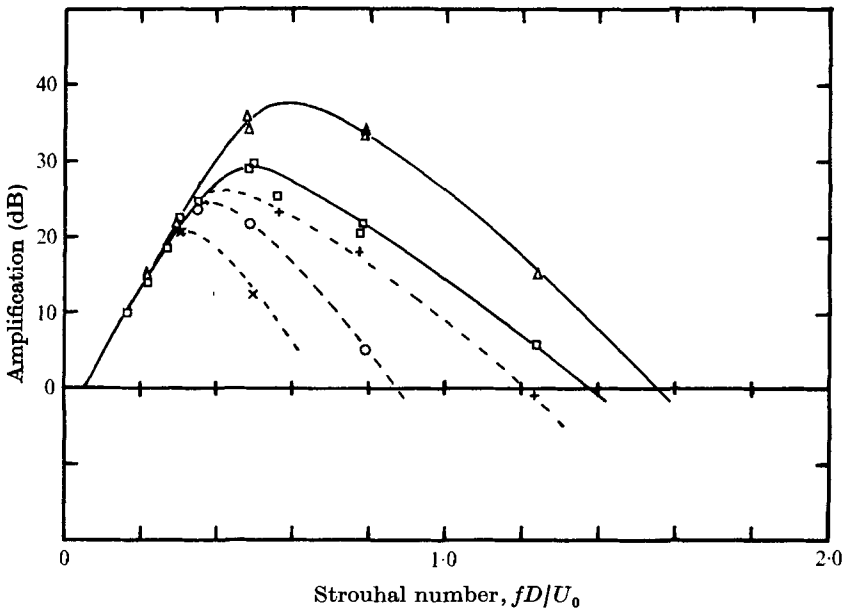

FIGURE 24. Variation of maximum centre-line amplification with Strouhal number. Linear range: △, fluctuating velocity; □, fluctuating pressure. Fluctuating pressure in nonlinear range: ×, 1281 Hz; ○, 2050 Hz; +, 3254 Hz.

than those measured by Crow & Champagne. However all their measurements seem to have been in the nonlinear range, which will be discussed in §4.

There are several theories available for calculating the behaviour of the instability wave. Michalke (1971*a*) obtains results for locally parallel shear flow. Chan (1974*a*, *b*, 1975) and Crighton & Gaster (1976) produce results for a divergent shear layer, but they are not qualitatively different locally from those of Michalke.

Figure 25 shows the variation of the velocity and pressure amplification rates and the phase speed with axial distance for $M = 0{\cdot}5$ and the three drive frequencies. Also shown on these curves are the theoretical variations produced by Chan for a Strouhal number of 0·5. The general forms of the curves agree well, but the measured amplification rate is smaller than that predicted and the agreement is poor at larger downstream distances where the shear layers start to merge and the instability wave decays.

The precise form of the theoretical curve depends on the shear-layer profile chosen for each axial position. The profiles assumed by Michalke and Chan are compared in figure 6 with the normalized measured profiles. Michalke's profile agrees well with measurements, but Chan assumes a much wider jet, which may contribute to the difference between his theory and the experimental results.

Since Michalke's profiles are so similar to the measured ones, comparison with his results may be more appropriate. He obtains the phase speed and amplification rate as a function of the Strouhal number based on the shear-layer momentum thickness θ and the ratio of the jet radius R to θ. By integrating the measured velocity profile, we can obtain the momentum thickness as a function of axial distance: $\theta = 0{\cdot}0335x$.

Michalke produces results for $R/\theta = 6{\cdot}25$ and 12·5, which correspond to axial distances of $x/D = 2{\cdot}38$ and 1·19 respectively, and measurements for different

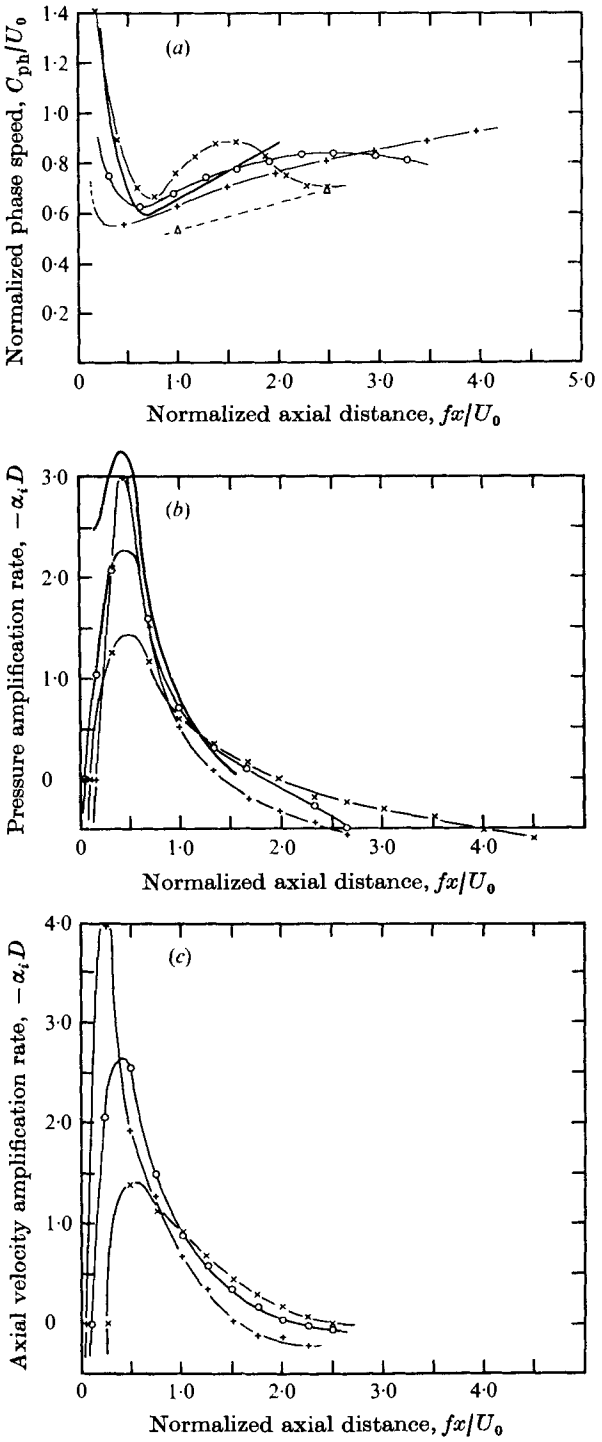

FIGURE 25. Axial variation of (*a*) phase velocity, (*b*) pressure amplification rate and (*c*) velocity amplification rate on jet centre-line at a jet velocity of $0{\cdot}49a_0$. Frequency: ×, 1281 Hz; ○, 2050 Hz (St = 0·48); +, 3254 Hz. ——, theory of Chan (1975) at St = 0·5; △, wave group velocity from schlieren photographs.

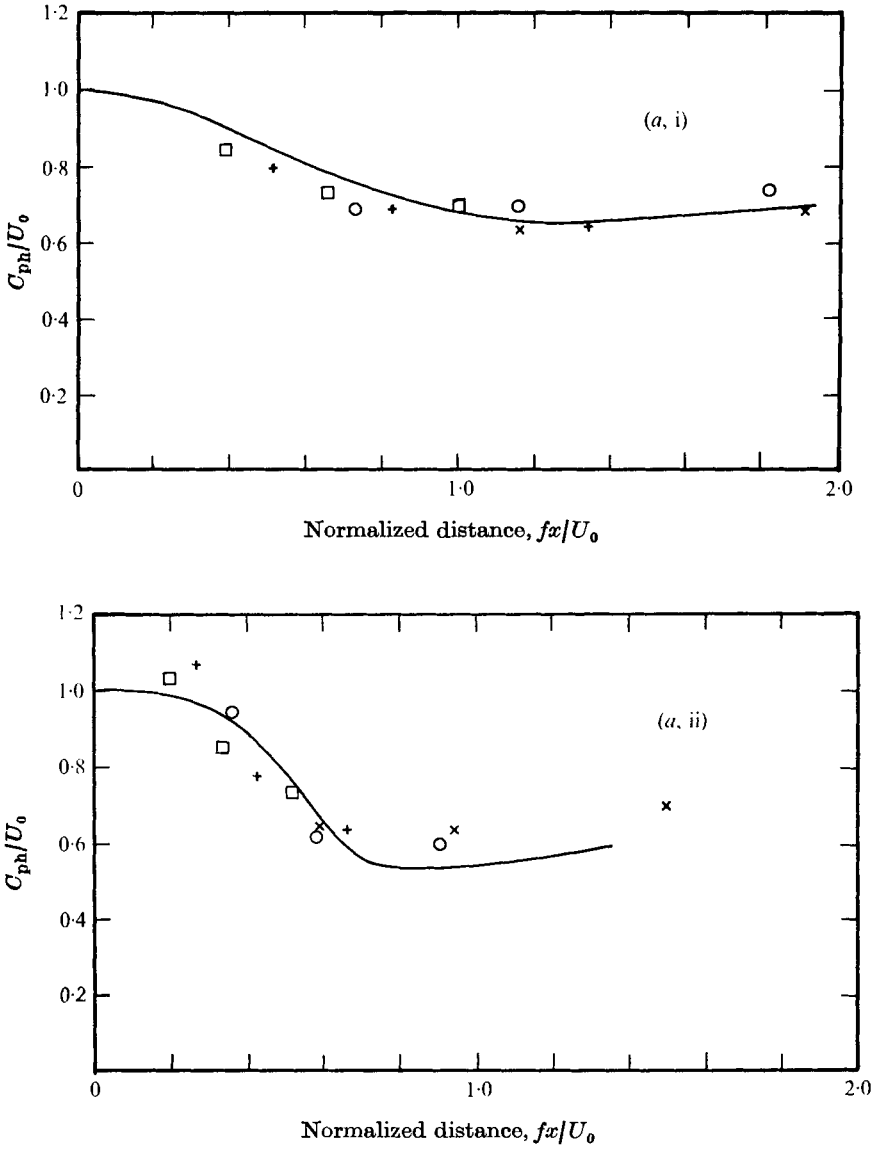

FIGURE 26 (*a*). For caption see next page.

frequencies and velocities are compared with his results in figure 26. The agreement of the phase speed is extremely good, although there are some points where the wave is moving faster than the mean flow. These waves are discussed by Bechert & Pfizenmaier (1975*b*).

Although the agreement of the amplification curves is extremely good over the rising region, none of the curves reaches the peak amplification rate as the curve for each velocity tends to flatten out at a different level and then decreases at a much lower rate than the theoretical curve for $R/\theta = 6{\cdot}25$. Michalke produces curves for different Mach numbers, which depart from the curve for zero Mach number to produce lower peak values as the Mach number increases. However the measured data do not follow

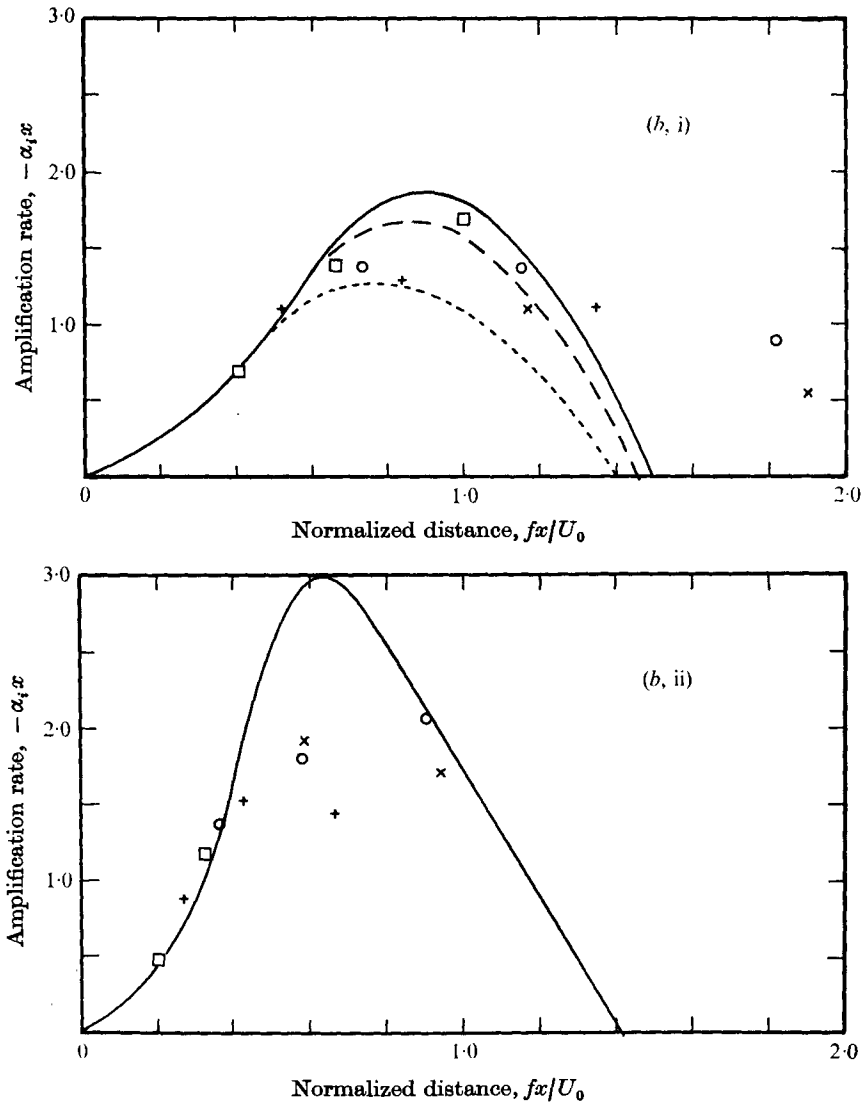

FIGURE 26. Comparison of (*a*) measured phase speed and (*b*) measured amplification rates with theory of Michalke (1971*a*). Data for (i) $R/\theta = 6{\cdot}25$, (ii) $R/\theta = 12{\cdot}5$. Data measured at jet velocities of: ×, $0{\cdot}3a_0$; ○, $0{\cdot}49a_0$; +, $0{\cdot}66a_0$; □, $0{\cdot}83a_0$. Theory: ——, $M = 0$; – –, $M = 0{\cdot}4$; - - - -, $M = 0{\cdot}8$.

these trends, the highest amplification rate being produced for the highest Mach number at $R/\theta = 6{\cdot}25$.

There are two other possible causes for the discrepancies. First, the calculations are for an inviscid shear layer. Pfizenmaier (1973) discusses the effect of a reduced Reynolds number and shows that there is a possible reduction of the peak amplification to half that of the inviscid case at a Reynolds number of 10^4. The Reynolds number of the measurements varied from $1{\cdot}3 \times 10^5$ to 10^6. The other possible cause of the variation of the curve with velocity is the effect of mean velocity on the shear-layer profile since the curves were obtained assuming the $M = 0{\cdot}3$ profile.

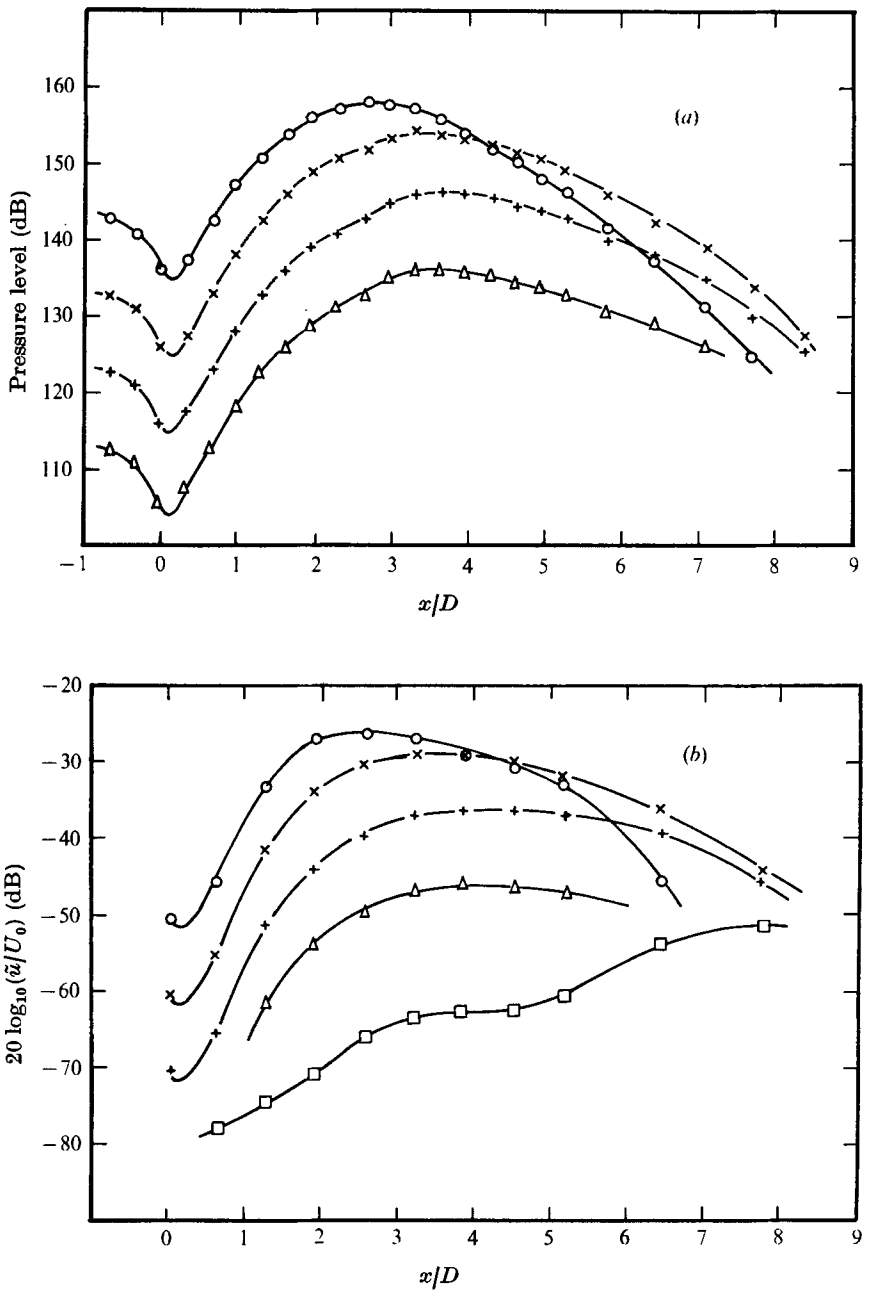

FIGURE 27. Effect of drive level on axial variation of (*a*) fluctuating pressure and (*b*) fluctuating velocity at a jet velocity of $0{\cdot}49a_0$ and frequency of 2050 Hz. ○, full drive; ×, 10 dB; +, 20 dB; △, 30 dB reduction of level; □, no excitation.

Although the basic behaviour of the instability wave is predicted by the linear theory in the linear amplitude range, the details are not represented by the present available theory.

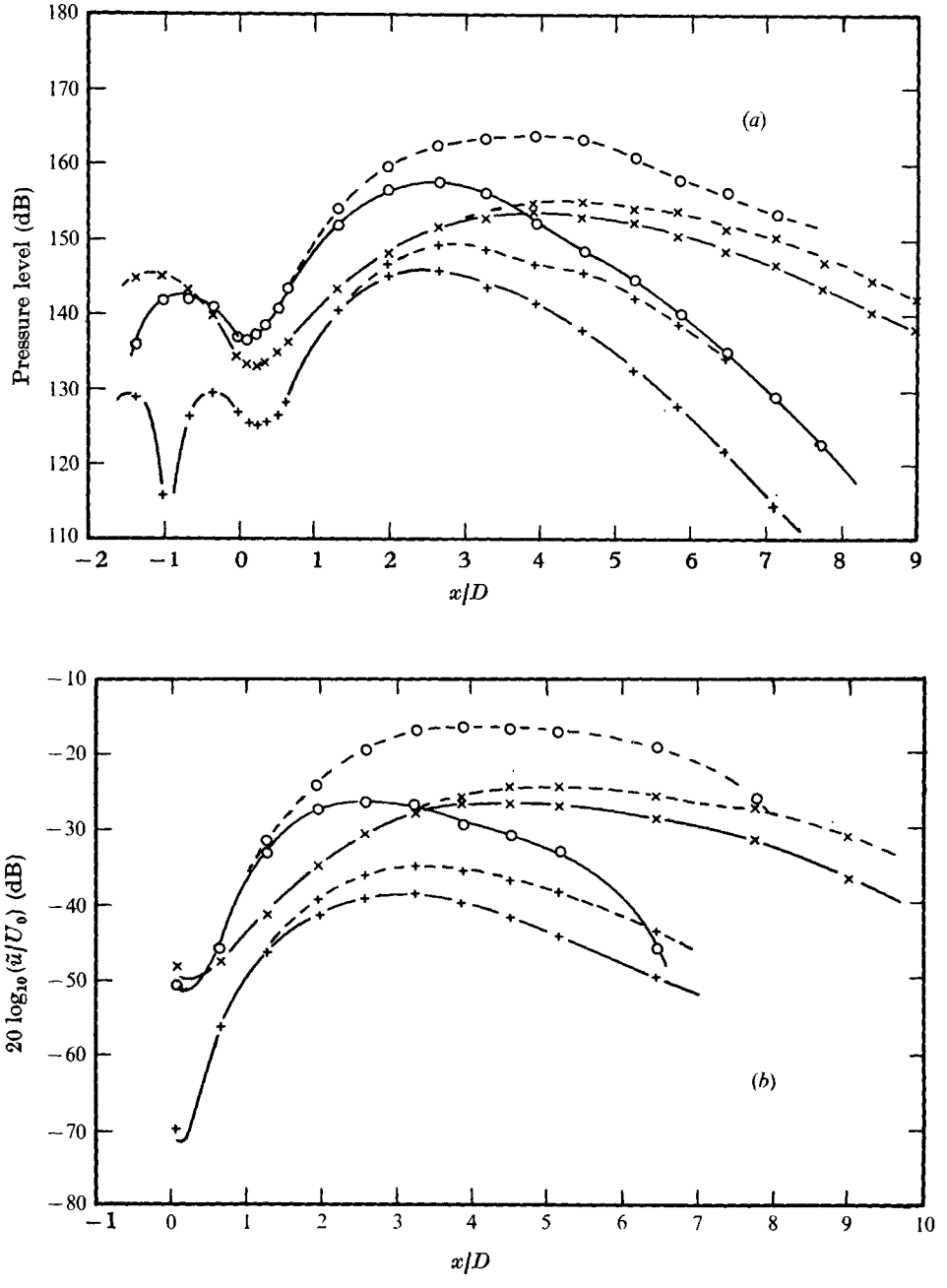

FIGURE 28. Comparison of axial variation of (*a*) fluctuating pressure and (*b*) fluctuating velocity at a jet velocity of $0{\cdot}49a_0$. Frequency: ×, 1281 Hz; ○, 2050 Hz; +, 3254 Hz. ——, maximum drive level; – – –, low drive level results linearly extrapolated to the high drive level.

4. High-level excitation

4.1. *The instability wave*

As the level of the excitation signal is increased beyond a certain level which depends on the mean velocity and frequency of excitation, the amplitude of the instability wave does not increase in proportion to the drive level. Figure 27 shows the axial variation of the pressure and velocity signals for various excitation levels at $M = 0{\cdot}5$, $f = 2050$ Hz. Close to the nozzle the behaviour is linear, but further downstream there is considerably less amplification at the higher excitation levels. At large distances downstream there is even a decrease in the measured level for an increase in excitation. Similar results are obtained for both velocity and pressure fluctuations, although the detailed variation is different.

Figure 28 shows the effect of the nonlinearity on the fluctuating pressure and velocity at the three test frequencies. In this case the variation at maximum drive level is plotted, together with the variation in the linear range at -30 dB, which has been linearly extrapolated upwards by 30 dB for comparison. The effect of the nonlinearity is to lower the peak of the amplification curve and move it back towards the nozzle by an amount which depends on the strength of the drive, the frequency of excitation and the mean velocity of the jet flow. Similar results for the fluctuating velocity were shown by Crow & Champagne (1971) although all their curves tended to merge at a large distance from the nozzle. This common level was probably the broad-band noise level, which for our experiment was filtered out, leaving only the instability wave.

Figure 24 shows the effect of the nonlinearity on the maximum amplification of the instability wave as a function of Strouhal number compared with that for linear excitation. There is little effect at the low Strouhal numbers but, as the Strouhal number increases, the nonlinear curve for each frequency leaves the curve for the linear range and reaches a lower maximum at a lower Strouhal number.

The typical effect of the nonlinearity on the phase relationships can be seen for the case $M = 0{\cdot}5$, $St = 0{\cdot}5$ in figures 21 and 23. The changes are small, with a slight increase in the phase velocity of the wave and an increased rate of change of relative phase angle with axial distance.

Figure 29 (plates 8–10) shows the variation of the averaged schlieren photographs of the jet with drive level for a range of flow velocities and frequencies of excitation. As the level increases, the form of the instability wave changes from a series of almost straight lines at approximately 45° to the jet axis to clearly repeated vortex rings of large cross-section, similar to those found by Brown & Roshko in a two-dimensional shear layer.

Similar effects occur at each frequency, the distance between vortices decreasing with an increase in frequency or a decrease in flow velocity. Only a few cycles of the disturbance are evident, which is in agreement with the axial shortening of the instability wave region shown by pressure and velocity measurements.

4.2. *Internal broad-band fluctuations*

A further effect of an increased excitation level is a change in the broad-band turbulence within the jet. This has been characterized by the spectra of the broad-band pressure fluctuation on the jet axis and is shown in figure 30 for a flow Mach number of

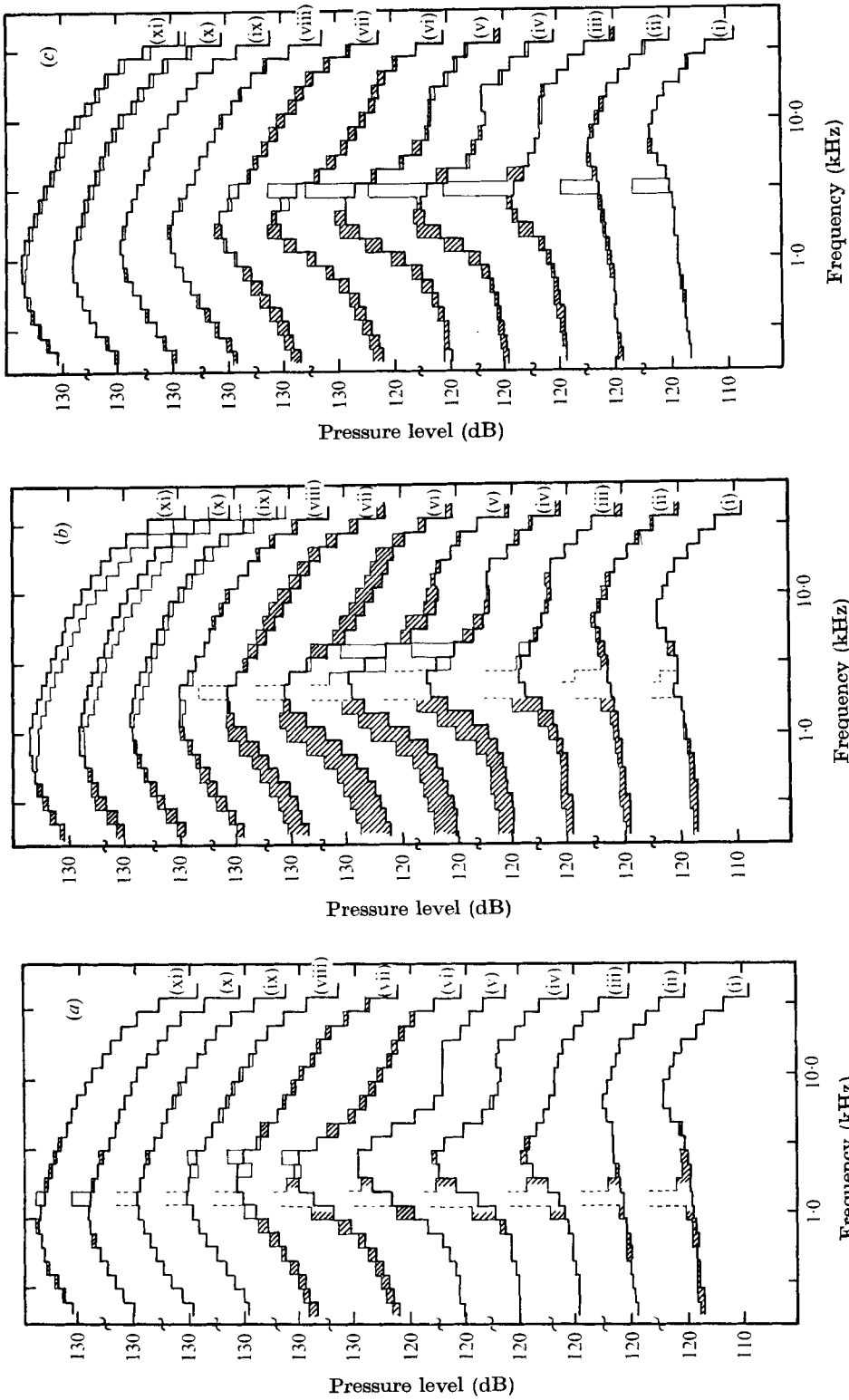

Figure 30. Axial variation of fluctuating pressure ⅓ octave spectra on centre-line of jet with (——) and without (——) excitation at (*a*) 1281 Hz, (*b*) 2050 Hz and (*c*) 3254 Hz. Shaded area shows increased level. Axial distances: (i) 0·06*D*, (ii) 0·65*D*, (iii) 1·29*D*, (iv) 1·94*D*, (v) 2·58*D*, (vi) 3·87*D*, (vii) 5·16*D*, (viii) 6·45*D*, (ix) 7·74*D*, (x) 9·03*D*, (xi) 10·32*D*.

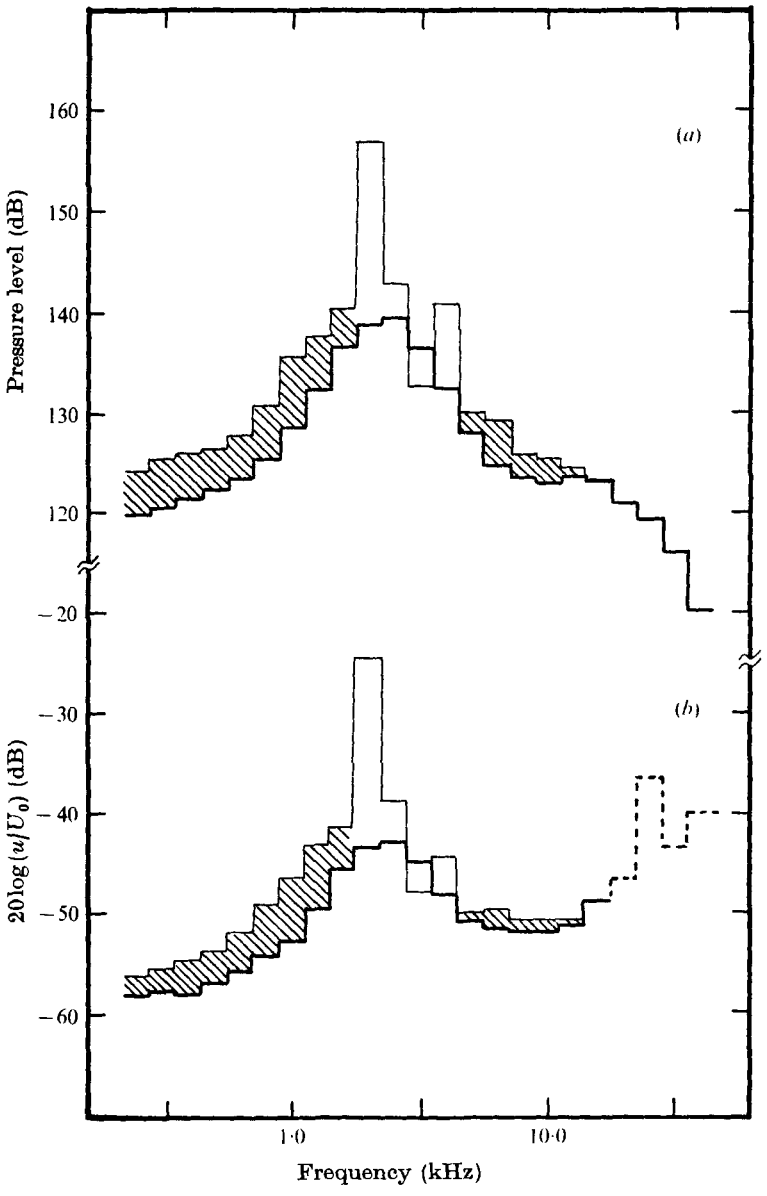

FIGURE 31. Comparison of (*a*) fluctuating pressure and (*b*) fluctuating velocity spectra on centre-line of jet at an axial distance of 2·58*D* with (——) and without (▬▬) excitation. Shaded area shows increase in level.

0·5 and the three test frequencies. The middle frequency of 2050 Hz corresponds to a Strouhal number of 0·5, which is in the region of maximum amplification of the instability wave. Similar signals were obtained for the fluctuating velocity, as shown in figure 31. The main frequency range of interest is below about 12 kHz; above this frequency much of the microphone signal is caused by turbulent fluctuations of the microphone boundary layer and some of the hot-wire signal is caused by wire vibration.

With 2050 Hz excitation, the broad-band fluctuations first increase at low frequencies as the distance from the nozzle is increased. Further downstream the higher frequency components increase and then decrease again until at about 7 diameters downstream their level is below the unexcited level. At large distances there is a very slight reduction in the peak level, but a significant shift of the peak to lower frequencies. The maximum increase in the spectrum is about 7 dB, which occurs approximately at the end of the potential core.

The higher frequency of excitation produces a similar trend, although the amplitude of the maximum excitation is smaller, producing a smaller increase in the broad-band turbulence. The lower frequency of excitation produces an increase only near the end of the potential core. However, under these conditions ($St = 0{\cdot}3$) the excitation is not great enough to produce significant nonlinearity as can be seen from figure 28 (*a*). The increase in broad-band fluctuations therefore appears to be linked to the nonlinear response of the shear layer.

4.3. *Description of nonlinear behaviour*

As the amplitude of the excitation increases, the amplitude of the motion of the shear layer caused by the instability wave increases. This increases the local instantaneous shear and hence increases the instantaneous rate of amplification of the small-scale turbulence. The turbulent amplification process drains energy from the instability wave into the broad-band turbulence. Excitation also increases the mean rate of spreading of the shear layer, and this increases the effective cross-sectional area of the mixing region and hence the integrated energy of the turbulence. These two mechanisms extract energy from the instability wave which has previously been extracted from the mean flow.

Several analyses of this process have been published, e.g. Liu (1974), Morris (1971) and Chan (1975). The last produces the results which are most directly applicable to the experimental results of the previous section. The analysis is performed by writing down the energy balances for the mean flow, instability wave and turbulence. Each energy balance contains production, diffusion and dissipation terms. The production term for the instability wave is found from locally linear instability theory and the turbulent production is found from the mean flow. The instability wave is modelled on an eddy-viscosity basis. Data are available for the one example given by Chan, for a Strouhal number of 0·5 at axial distances of up to three diameters, and the comparison is shown in figure 32.

The results for the behaviour of the instability wave agree quite well with the theory. An estimate of the drive energy at the highest excitation level is 10^{-5} times the mean flow energy, and the corresponding curve falls between the calculated results of Chan for energies of 10^{-6} and 10^{-4}. The broad-band variation of the measured energy on the centre-line and the calculated energy integrated across the jet show the same trend, but the calculated values are smaller than those measured. This could be caused by comparison of radially integrated and centre-line energies, but it is most probable that this would cause the measured values to be smaller than those calculated.

It may be that the essentially linear theory is not adequate to predict the detailed behaviour of the wave, and the discrepancy would be even greater further downstream, where the behaviour of the wave is not accurately predicted even in the linear range. A

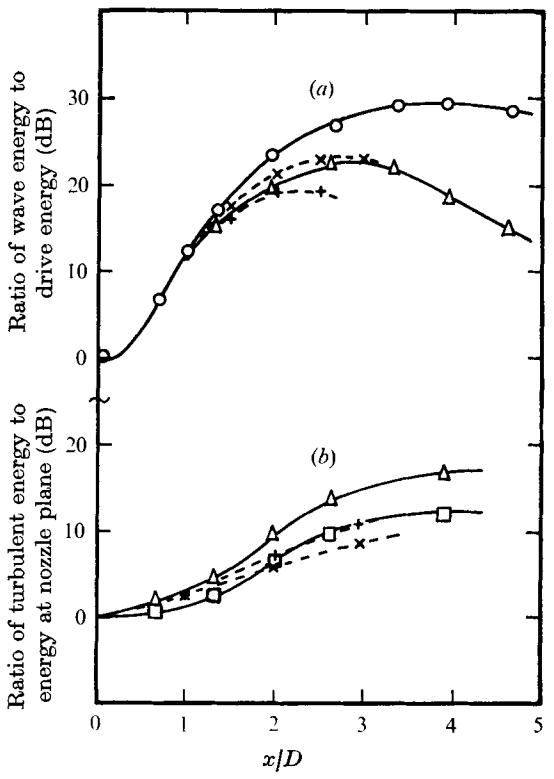

FIGURE 32. Comparison of axial variation of measured amplification of (*a*) instability wave energy and (*b*) turbulence energy with theory of Chan (1975). Measured data: □, no drive; △, maximum drive level (relative energy 10^{-5}); ○, 30 dB below maximum drive. Theory for energy of: ×, 10^{-6}; +, 10^{-4}.

more promising approach may be numerical analysis of the instability wave such as those produced by Grant (1974) and Acton (1976). These calculations show shear-layer developments very similar to those obtained by flow visualization. Individual vortices, however, have a ragged appearance and also tend to lose small portions, which could correspond to the generation of broad-band fluctuations.

5. Far-field noise

The far-field noise of the jet is modified in two ways when the jet is excited by internal sources: the excitation signal is radiated, and the broad-band noise is modified by a change in turbulent structure. The excitation signal is radiated directly from the nozzle, but could also be amplified by radiation from the instability wave. The broad-band noise modification, independently discovered by Bechert & Pfizenmaier (1975*a*) and at Rolls-Royce Advanced Research Laboratory, will be described first.

5.1. *Broad-band noise modification*

Some examples of the effect on the OASPL of the broad-band noise for excitation at two frequencies are shown in figure 33 as a function of angular position and flow speed. The excitation tone and its harmonics have been electronically rejected from the

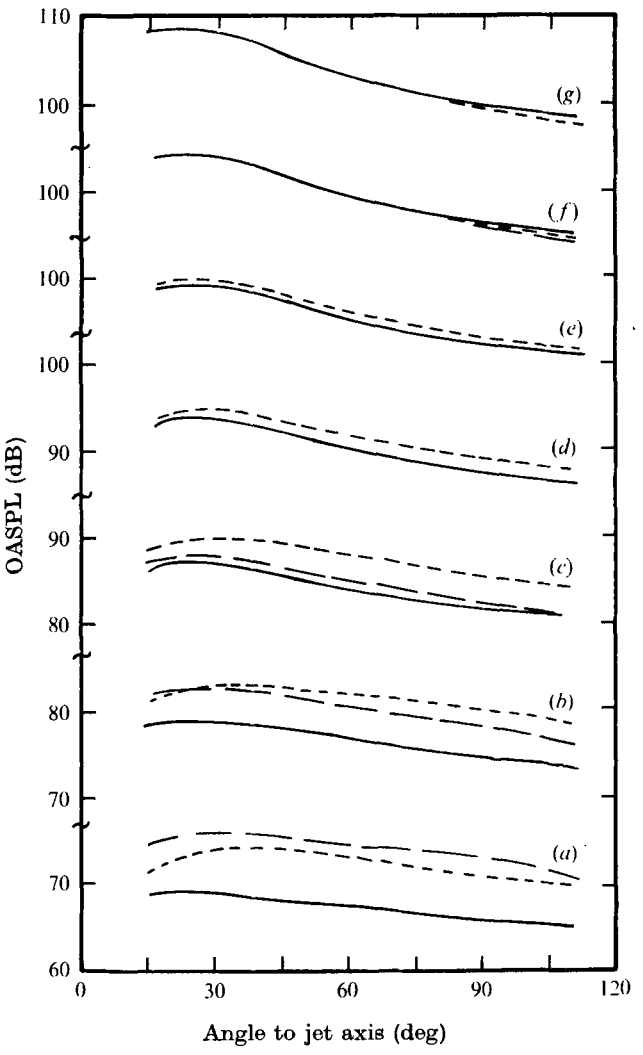

FIGURE 33. OASPL far-field directivity of jet broad-band noise with jet velocity of (*a*) $0{\cdot}3a_0$, (*b*) $0{\cdot}39a_0$, (*c*) $0{\cdot}49a_0$, (*d*) $0{\cdot}58a_0$, (*e*) $0{\cdot}66a_0$, (*f*) $0{\cdot}75a_0$ and (*g*) $0{\cdot}83a_0$. Maximum level of excitation at: — —, 1281 Hz; – · – ·, 2050 Hz. ——, levels of unexcited jet.

measured signal. The field shapes are very similar to those of the unexcited jet noise, but the level depends on jet velocity and excitation frequency. These results have been replotted in figure 34 as a function of jet velocity and show trends which are remarkably similar to those of excess noise.

The frequency analysis of the results for $M = 0{\cdot}5$ is shown in figure 35. Again the directivity at each frequency remains nearly constant, but the relative level changes. At high frequency, for angles close to the jet axis the shape of the curve is slightly modified, showing an increase in the width of the cone of silence, probably because the changed spreading rate of the jet affects refraction. These results are shown more clearly in terms of spectra (figure 36). Those with excitation have steeper peaks than those of the unexcited jet and the frequency of the peak varies with excitation fre-

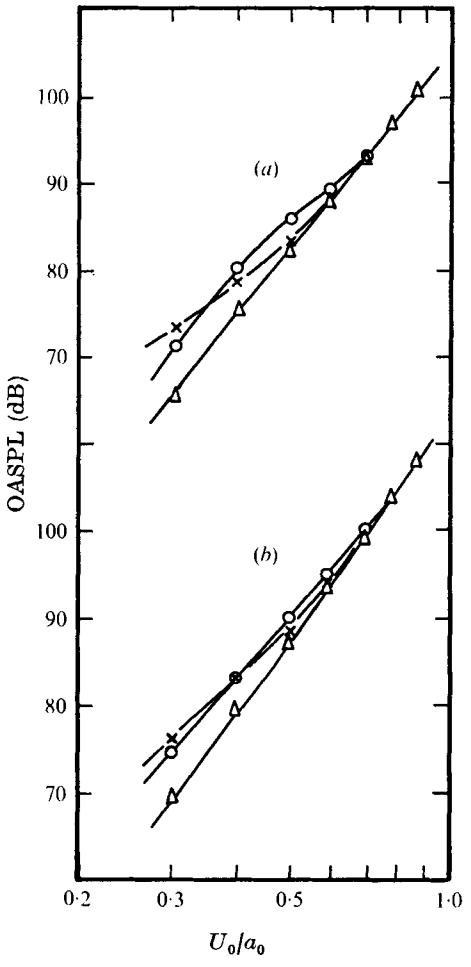

FIGURE 34. Variation of jet broad-band noise with jet velocity at full excitation level. Frequency: ×, 1281 Hz; ○, 2050 Hz. Comparison with results for no excitation (△) at angles to jet axis of (*a*) 90° and (*b*) 30°.

quency, but not with flow speed as does pure jet noise. At 30° to the jet axis, the peak of the spectrum is at approximately the same frequency as the tone. At larger angles the peak occurs at frequencies up to half an octave higher.

The variation of the broad-band noise with the level of excitation has been measured at 60° to the jet axis at excitation frequencies between 0·8 and 10 kHz. The results depend strongly on the jet velocity and excitation frequency and show decreases as well as the increases reported by Bechert & Pfizenmaier (1975*a*). Typical results are shown in figure 37 and can be approximately characterized for each jet condition by the slope of the asymptotic straight line at high levels and the intercept with the broad-band noise level of the unexcited jet.

The slope or sensitivity is shown in figure 38 as a function of Strouhal number and Mach number. Below a Mach number of 0·7 the behaviour is only weakly dependent on Mach number, all results collapsing onto a single curve with a peak increase at a Strouhal number of 0·35 and a decrease for Strouhal numbers greater than 1·5. This

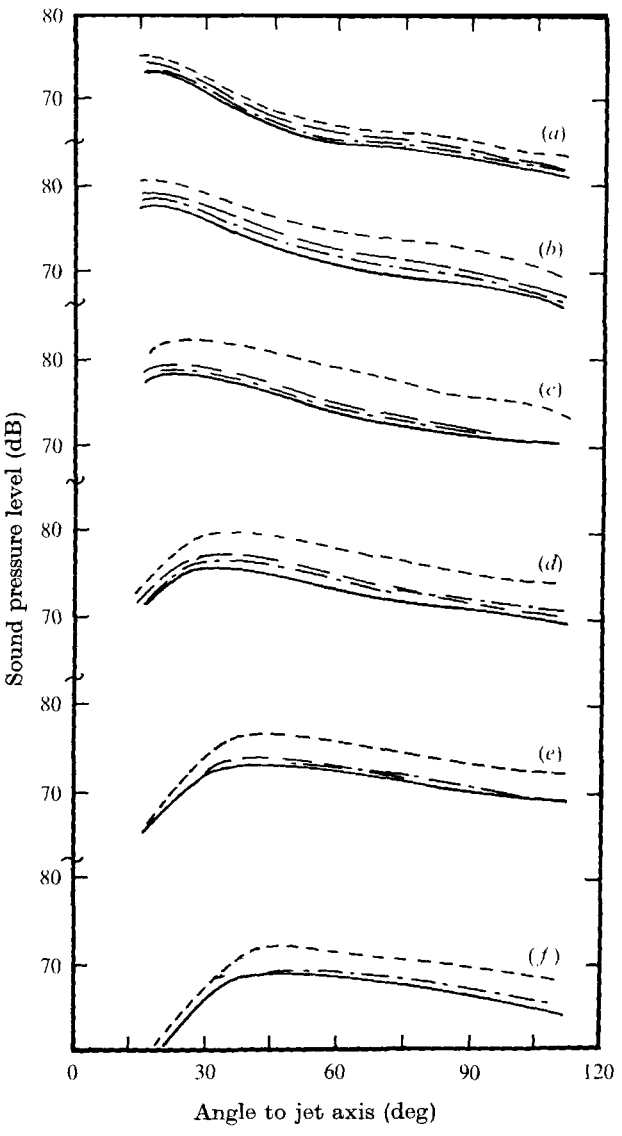

FIGURE 35. Comparison of $\frac{1}{3}$ octave filtered field shapes of broad-band noise in far field of jet at a jet velocity of $0{\cdot}49a_0$. ——, without excitation; — —, excitation at 1281 Hz; - - - -, excitation at 2050 Hz; —·—, excitation at 3254 Hz. Third octave centre-frequencies: (*a*) 500Hz, (*b*) 1 kHz, (*c*) 2 kHz, (*d*) 4 kHz, (*e*) 8 kHz, (*f*) 16 kHz.

result might be expected from the results of Vlasov & Ginevskiy (1974) on the effect of external acoustic excitation on the internal turbulence of a jet. At higher Mach numbers the peak sensitivity falls, staying at approximately the same Strouhal number. Although the behaviour in this region is less certain because higher-order acoustic modes can propagate more readily in the duct, the uniqueness of the behaviour with Mach number indicates that this is probably an effect of compressibility.

The behaviour of the intercept or threshold has to be expressed in terms of an absolute measured parameter at some position. The most useful jet parameter was found

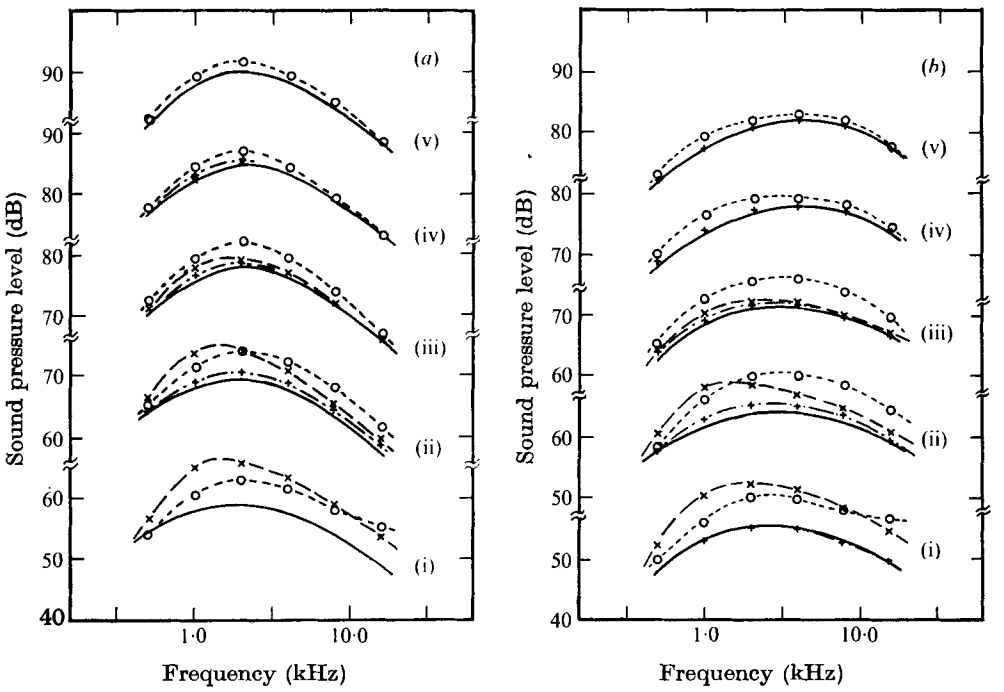

FIGURE 36. Spectra of broad-band sound pressure level in far field of jet at (*a*) 30° and (*b*) 90° to the jet axis and at jet velocities of (i) $0{\cdot}3a_0$, (ii) $0{\cdot}39a_0$, (iii) $0{\cdot}49a_0$, (iv) $0{\cdot}58a_0$ and (v) $0{\cdot}66a_0$. ——, natural broad-band level. Levels at full excitation: — —, 1281 Hz; – – – –, 2050 Hz; — · —, 3254 Hz.

to be the sound pressure level measured in the nozzle plane. The results are plotted in figure 39 normalized with respect to the minimum threshold at each Mach number. The results collapse well, showing no dependence on Mach number. The behaviour of the minimum threshold level is shown in figure 40 as a function of jet dynamic head. The minimum occurs at a Strouhal number of approximately 0·7 and represents an r.m.s. sound pressure of 0·08 % of the dynamic head. There is a departure from this at high Mach numbers, again probably caused by compressibility effects.

There is also a departure from this behaviour at Mach numbers below 0·3, where the threshold rises steeply for decreasing Mach number. At these low velocities the unexcited jet noise no longer follows the eighth power of velocity and some noise caused by upstream valves appears in the spectra. It is probable that this noise excites the instability wave sufficiently to increase the jet noise. This means that a very much higher excitation level is required to further increase this already augmented broad-band level.

All the previous data have been for tone excitation of the instability wave. Similar effects occur for broad-band excitation. Figure 41 compares the broad-band noise increases when broad-band acoustic excitation is applied. Curve (*a*) shows the spectra for tone excitation at 2050 Hz. Curve (*b*) shows the results for a 30 Hz band of random noise. The bandwidth is increased to 300 Hz for curve (*c*) and to 2 kHz for curve (*d*). As the bandwidth increases, the r.m.s. value of the acoustic excitation signal decreases since the frequency response is not flat and the input electrical signal is limited to a

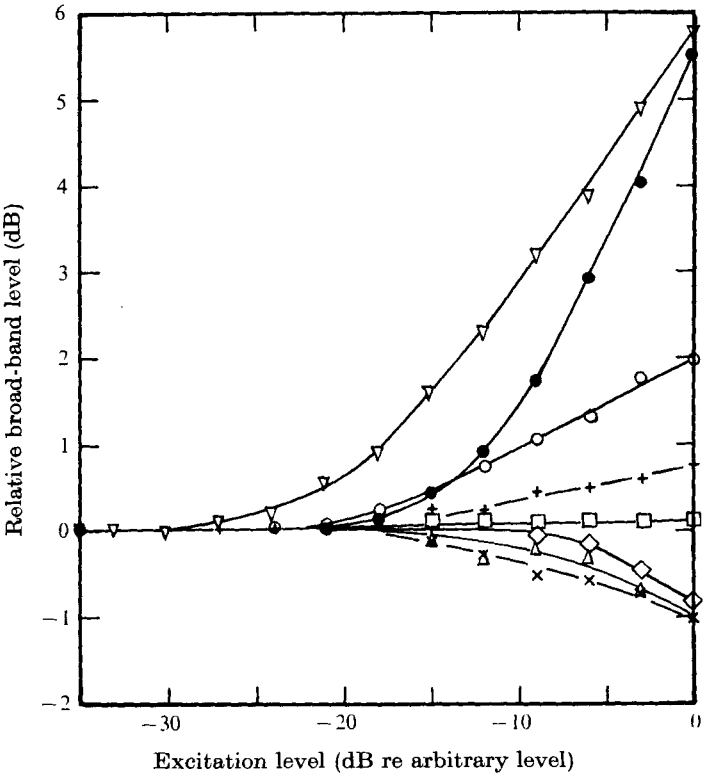

FIGURE 37. Examples of sensitivity to drive level of OASPL of broad-band radiated noise at a jet velocity of $0{\cdot}4a_0$. Frequency: ▽, 1281 Hz; ●, 1855 Hz; ○, 3155 Hz; +, 4088 Hz; □, 5203 Hz; ×, 7518 Hz; ◇ 8728 Hz; △, 10516 Hz.

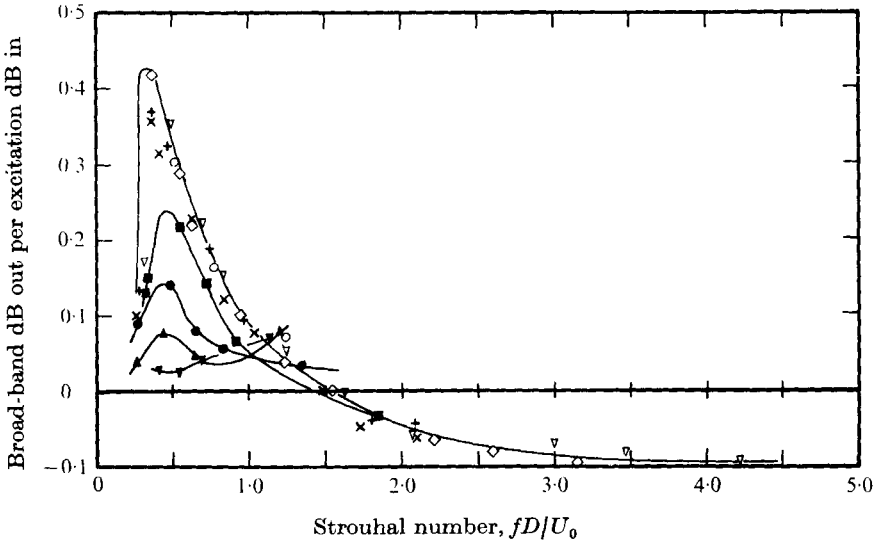

FIGURE 38. Variation of sensitivity of broad-band modification with Strouhal number. Mach number: ○, 0·2; ▽, 0·3; ◇, 0·4; +, 0·5; ×, 0·6; ■, 0·7; ●, 0·8; ▲, 0·9; ▼, 1·0.

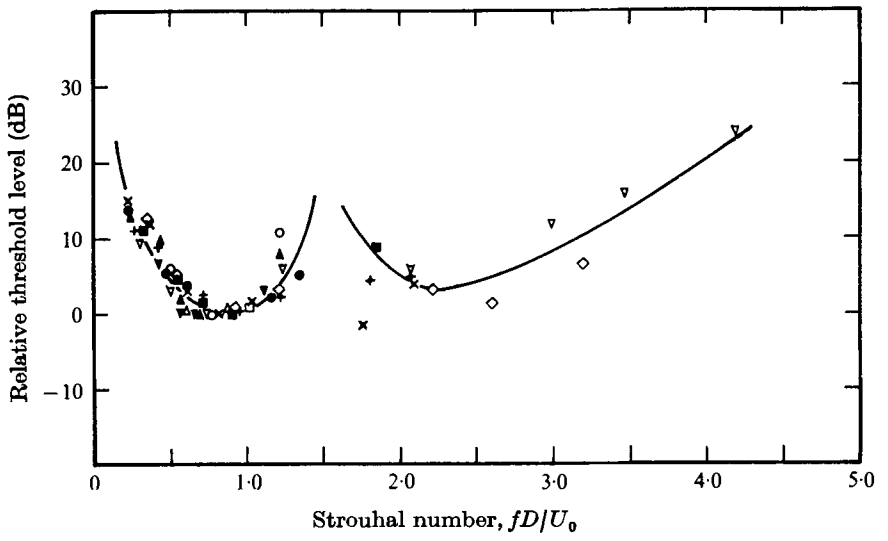

FIGURE 39. Variation of threshold excitation level with Strouhal number and Mach number. Symbols as for figure 38. Curve for each Mach number normalized by minimum value.

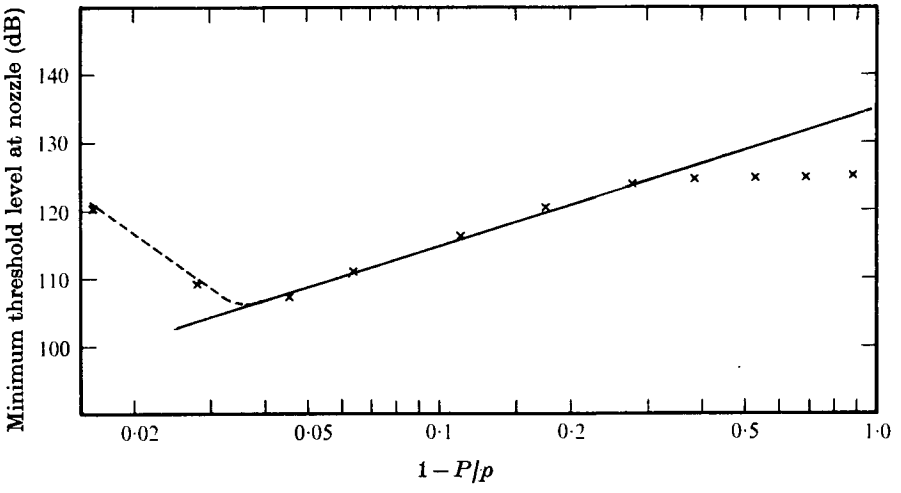

FIGURE 40. Variation of minimum threshold level in nozzle exit plane with jet dynamic head. ——, r.m.s. pressure of 0·08 % of dynamic head.

constant r.m.s. value. Despite this decrease in drive level compared with that for tone excitation, there is still a considerable increase in the broad-band noise outside the frequency range of the excitation signal.

The level of excitation required, a 0·08 % pressure fluctuation, is very small compared with the percentage of turbulence measured in the nozzle plane. However, in order to excite the instability wave these fluctuations must be laterally correlated. This occurs naturally with acoustic excitation, but measurements have shown that only about 1 % of the turbulent energy is correlated. If, however, turbulent or thermal fluctuations were sufficiently correlated it is probable that they would be just as effective in exciting the instability wave and increasing the broad-band noise.

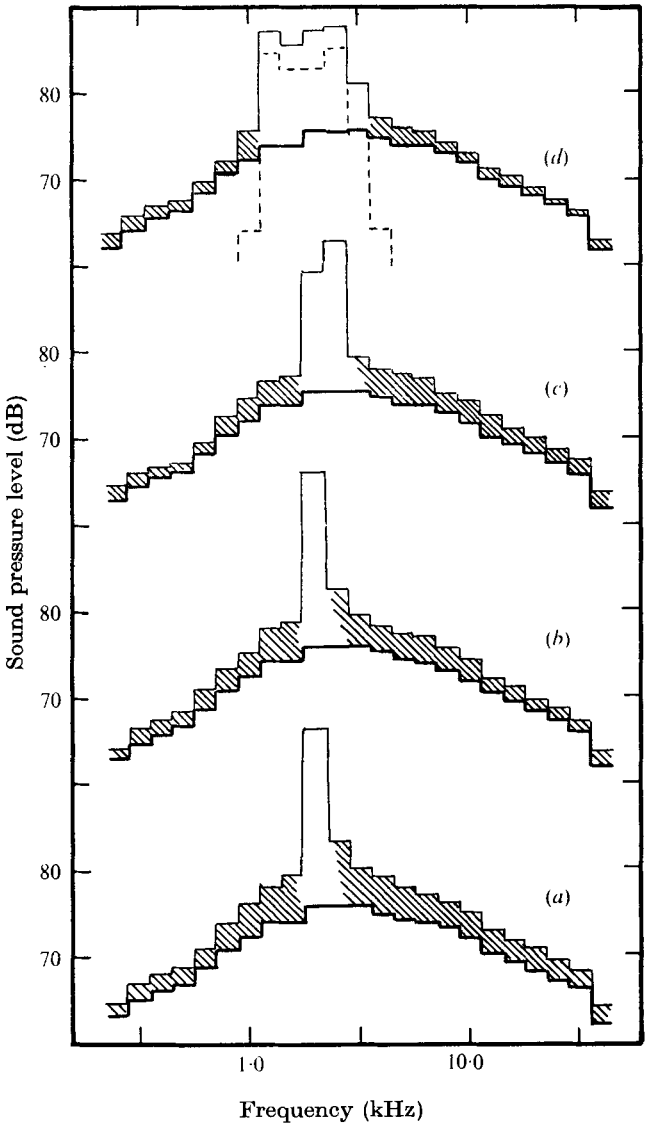

FIGURE 41. Comparison of far-field spectra (——) with and (——) without excitation at 60° to jet axis and at a jet velocity of $0{\cdot}49a_0$ as bandwidth of excitation signal is increased. (*a*) Pure-tone excitation. (*b*) 30 Hz bandwidth random excitation. (*c*) 300 Hz bandwidth random excitation. (*d*) Random excitation in band from 1 kHz to 3 kHz. – – – –, excitation spectrum.

5.2. *Radiation of excitation signal*

It has been suggested by Crow (1972) and supported by some calculations of Crighton (1975) that significant acoustic power is radiated by the instability wave in the subsonic velocity range. Such radiation from instability waves was established by, for example, McLaughlin, Morrison & Troutt (1975), Liu (1974), Bishop *et al.* (1971) and Mattingly & Chang (1974), for jets where the motion of the instability wave is supersonic, but no detailed experimental evidence exists for subsonic conditions. The

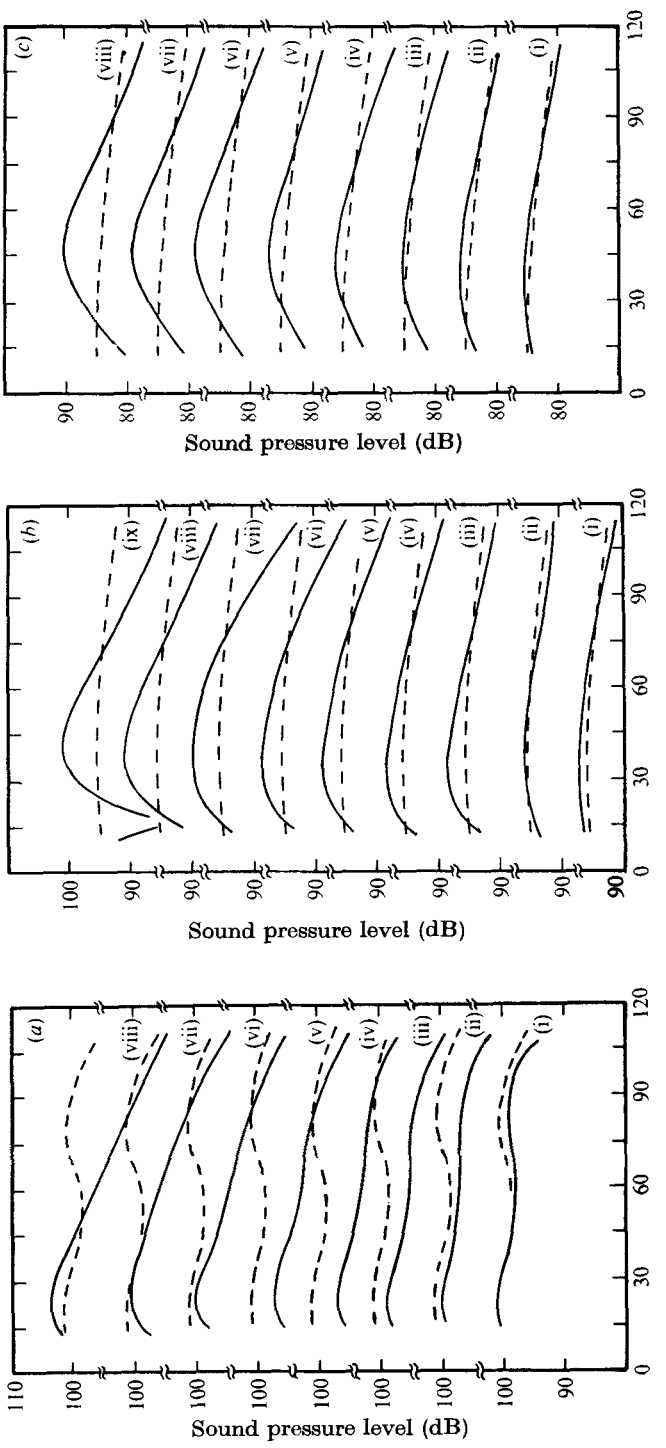

FIGURE 42. Variation of directivity of excitation tones at (*a*) 1281 Hz, (*b*) 2050 Hz and (*c*) 3254 Hz with jet velocity of (i) $0{\cdot}1a_0$, (ii) $0{\cdot}2a_0$, (iii) $0{\cdot}3a_0$, (iv) $0{\cdot}39a_0$, (v) $0{\cdot}49a_0$, (vi) $0{\cdot}58a_0$, (vii) $0{\cdot}66a_0$, (viii) $0{\cdot}75a_0$ and (ix) $0{\cdot}93a_0$. – – –, directivity with no flow.

radiation from the instability wave would be seen as an increase in the total acoustic power radiated to the far field at the excitation frequency and the jet could therefore be regarded as an amplifier of the internal noise.

The effect of flow on the field shapes of the excitation-tone radiation is shown in figure 42. These have been smoothed by eye to eliminate the slight standing waves caused by the imperfectly anechoic conditions. At the two higher frequencies there is a considerable increase in the peak radiated tone level at about 45°, but also a considerable reduction at angles greater than about 75°. The increase cannot be regarded as a true amplification, but may be simply the effect of refraction in the shear layer (Liu & Maestrello 1975; Schubert 1972).

The simplest test for amplification is to measure the total power passing through the duct and compare it with the total radiated power. The radiated power is given by

$$P = \frac{2\pi R^2}{\rho_0 a_0} \int_0^\pi p^2 \sin\theta \, d\theta.$$

This has been evaluated by splitting the directivity curves into 10° increments and summing the power in each band. The extra power radiated in the forward arc is estimated from the slope of the curve at 110°, but the correction is small.

Since only the plane wave is present inside the duct, the acoustic power transfer can be obtained from measurements on the duct centre-line. As seen in §3.1, there are large standing waves in the duct, so that the positively and negatively travelling pressure waves are nearly equal in amplitude. From Morfey (1970) the net power transferred along the duct is

$$P = (A/\rho_0 a_0)[p_+^2 (1+M)^2 - p_-^2 (1-M)^2].$$

We can express p_+ and p_- in terms of the measurable quantities on the duct centre-line, which are $p_{\max}$ and $p_{\min}$, i.e.

$$P = (A/\rho_0 a_0) p_{\max}^2 [(1+M^2)\gamma + (1+\gamma^2) M],$$

where γ is $p_{\min}/p_{\max}$ and can be positive or negative depending on whether the positively or negatively travelling pressure wave has the higher amplitude. The sign of γ is obtained from the direction of the phase-angle change as the probe passes through the minimum position. Since the positive and negative waves nearly cancel there, the direction of the phase change is that of the larger wave.

In most cases the pressure wave travelling upstream is larger than the one travelling downstream, but in all cases the net flow of power is positive and remains nearly constant. This means that the pressure reflexion coefficient is often greater than unity, although the power reflexion coefficient remains less than unity and decreases greatly as the flow speed increases. In most cases γ is very small, so that $p_+ \simeq p_-$, and the ratio of the upstream power to the downstream power is given by $(1-M)^2/(1+M)^2$. We can now see the reason for the fall in the pressure wave in the duct as the flow speed is increased. Since the plenum chamber is large the source will effectively be radiating a constant acoustic power in the direction of the duct entry. To keep this power constant for increased flow, the pressure amplitude must fall.

The far-field and internal acoustic power measurements are compared in figure 43. At the two higher frequencies the difference is always less than 1 dB, which is of the order of the experimental error. At the lowest frequency there is a reduction in acoustic power of up to 5 dB over part of the velocity range.

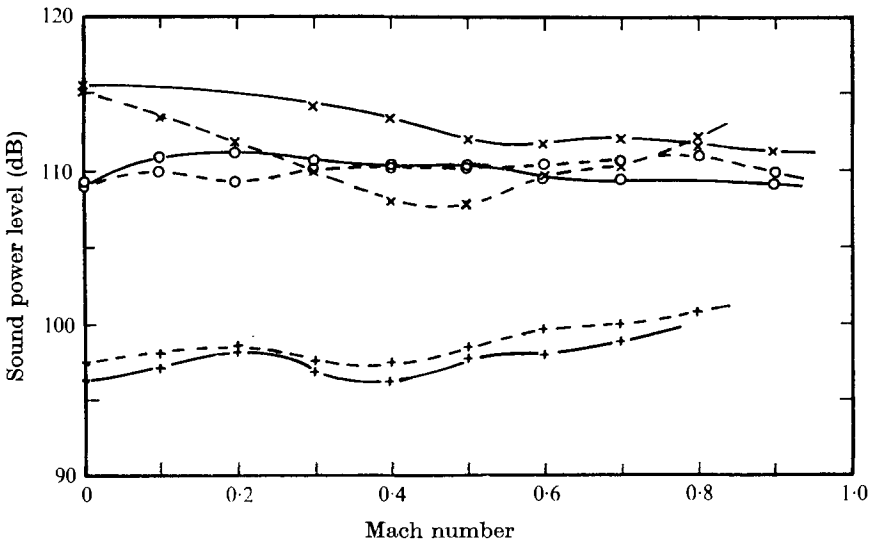

FIGURE 43. Variation of (——) in-duct and (– – –) far-field sound power with Mach number. Frequency: ×, 1281 Hz; ○, 2050 Hz; +, 3254 Hz.

These results indicate that there is no significant radiation from the instability wave over the Mach number range 0·1–0·9 and the Strouhal number range 0·1–3·5. A further piece of evidence for this is the fact that, although the instability wave has a nonlinear behaviour, the radiation to the far field is directly proportional to the excitation level. If the instability wave radiated significantly, the effective amplification of the jet would be expected to decrease as the level increased owing to both a decrease in the instability wave's relative amplitude and a decreased length of source. It is possible that the apparent amplification of the excitation reported by Crow (1972) was the result of the refraction of the wave by the shear layer, far-field standing waves in the measuring environment and the change in the power from the resonant source as it was tuned for the different flow conditions.

6. Discussion and conclusions

The results presented in the previous sections show clearly that large-scale jet structure plays an important part in the generation of jet noise. In the unexcited jet, it controls the mixing with the ambient air and hence controls the production of turbulence and noise. The instability waves are excited by acoustic, turbulent or thermal fluctuations in the jet flow and by feedback from previous waves. The waves are present in the form of zero-, first- and probably higher-order azimuthal modes as described, for example, by Michalke (1971*a*).

When the jet is artificially excited by a low-level acoustic source, the instability wave tends to lock onto it and produce a response which is in agreement with linear shear-layer instability theory. At higher excitation levels the wave extracts considerable energy from the mean flow and the response becomes nonlinear as some of this energy is converted to turbulent energy, which changes the jet turbulent structure and the jet noise. In a subsonic jet the shear layer does not radiate significant energy by

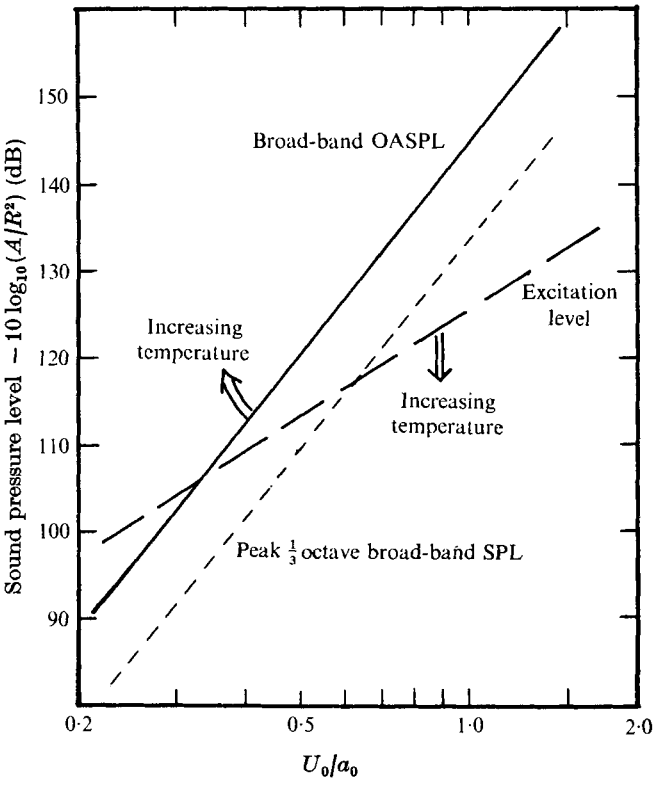

FIGURE 44. Comparison of threshold excitation level in far field at 60° to jet axis with unexcited broad-band jet noise at the same position.

itself, although such radiation does become important for supersonic jets as shown, for example, by Bishop *et al.* (1971), McLaughlin *et al.* (1975) and Liu (1974).

The most important result for the subsonic jet is the change in the radiated jet noise. This should not be regarded as a new source of noise, but simply as a modification of the Lighthill mixing noise. The traditional eighth-power variation with velocity and its refinements are based on simplified models for the mixing process and cannot be expected to predict the noise if the turbulent structure is changed as it is by the instability wave in this case. When regarded from this point of view, the wide scatter in both levels and spectra obtained for jet noise by different experimenters on different rigs becomes explicable, since even the best rigs have some internal disturbances. The level of disturbance required is very low, especially at low jet velocities, where the largest discrepancies occur.

In figure 40 it is shown that the level of acoustic excitation required for the threshold increase in broad-band noise is only 0·08 % of the jet dynamic head. This means that the threshold intensity level varies as the fourth power of jet velocity. If this level is projected to the far acoustic field, the approximate comparison with far-field natural jet noise shown in figure 44 is obtained. This shows that although the excitation tone is dominant at low velocities it is hardly discernible in the overall level or even in a $\frac{1}{3}$-octave spectrum at higher velocities. We have no direct evidence for the effect of jet temperature on the threshold level, but since the effect is governed by a hydrodynamic

instability it is probable that the threshold will depend only on the pressure fluctuation, and we have some data on large-scale hot rigs which support this. This means that as the temperature rises the threshold level in figure 44 falls and appears even less significant compared with the natural jet noise.

An acoustic tone or broad-band source can therefore change the jet noise significantly without being measured in the far field. Since the instability wave does not radiate significant acoustic energy, turbulent, thermal or vibrational excitation of the jet would also not be heard acoustically even at low jet velocities. Over the whole range of jet conditions it is possible to propose a source of excitation which would not be obvious in the noise signal and yet would change the jet structure and the radiated jet noise.

In a jet engine there are many possible sources of excitation. The combustion chamber can produce large thermal, acoustic and turbulent fluctuations which can be modified and augmented by the turbine. Turbulent and acoustic fluctuations can be produced by flow separation or eddy shedding from exhaust struts or centre-bodies. Any of these sources could excite the jet and modify the noise if sufficient energy was present in the correct Strouhal number range. There are no detailed measurements available on engines, but measurements of fluctuating velocity (Smart & Moore 1976) show turbulence intensities between 3 and 10%, which, even if not correlated across the nozzle plane, are probably sufficient to modify the basic jet noise. This means that excess noise sources in engines may be not only internally generated noise, but also the subsequently increased jet noise.

We have discussed the modification of the jet noise by shear-layer excitation and must now ask what role the instability wave plays in the unexcited jet. The instability wave and vortex formation and pairing mechanisms are definitely present in the natural jet and the disturbance spacing represents the correct Strouhal number range for maximum amplification. Also, this Strouhal number range around 0·5 corresponds to the peak of the natural jet noise spectrum, indicating a possible link between the noise and the jet structure. However considerably more work is necessary to determine the precise connexion between them.

In the high-speed schlieren photographs some of the disturbances on the shear layer were very much larger than others and these could be large enough to produce nonlinear effects and so increase the jet noise above the possible minimum. It would therefore appear that, by reducing the size and amplitude of these disturbances, the jet noise can be reduced. This may be the mechanism by which the high Strouhal number excitation reduces the noise; it effectively breaks up the large eddies before they can be amplified sufficiently to produce much broad-band noise. There will be a limit on the amount of reduction of the large-scale structure which can be attained, since it is an integral part of the mixing process and in the absence of nozzle forcing would probably be self-exciting.

A further means of reducing the effect of the instability wave would be to provide a shear-layer profile of a form which will not amplify the instability wave. Chan & Templin (1975) showed that such waves do not grow on a jet with an approximately Gaussian velocity profile at the nozzle plane produced by upstream gauzes. We should expect that such a nozzle, or any other with a smooth velocity profile, would not be sensitive to internal excitation. This may be the action of some silencer nozzles such as the coaxial-ring silencer described by Scharton & White (1972).

Most of the experimental results described in this paper were obtained by Mr D. H. Brierley, who also developed the flow-visualization system under the guidance of Dr A. E. Smart. The work was financially supported under a contract from the Ministry of Defence.

REFERENCES

ACTON, E. 1976 Modelling of large eddies in a two-dimensional shear layer. *J. Fluid Mech.* **76**, 561–592.

AHUJA, K. K. 1972 An experimental study of subsonic jet noise with particular reference to the effects of upstream disturbance. M.Phil. thesis, Q.M.C. London University.

AHUJA, K. K. 1973 Correlation and prediction of jet noise. *J. Sound Vib.* **29**, 155–168.

ARNDT, R. E. A. & GEORGE, W. K. 1974 Investigation of large scale coherent structure in a jet and its relevance to jet noise. *N.A.S.A. Contractor Rep.* no. 138908.

BECHERT, D. & PFIZENMAIER, E. 1975*a* On the amplification of broadband jet noise by pure tone excitation. *J. Sound Vib.* **43**, 581–587.

BECHERT, D. & PFIZENMAIER, E. 1975*b* On wavelike perturbations in a free jet travelling faster than the mean flow in the jet. *J. Fluid Mech.* **72**, 341–352.

BISHOP, K. A., FFOWCS WILLIAMS, J. E. & SMITH, W. 1971 On noise sources of the unsuppressed high speed jet. *J. Fluid Mech.* **50**, 21–30.

BRADSHAW, P., FERRISS, D. M. & JOHNSON, R. F. 1964 Turbulence in the noise producing region of a circular jet. *J. Fluid Mech.* **19**, 591–624.

BROWN, G. L. & ROSHKO, A. 1974 On density effects and large-scale structures in turbulent mixing layers. *J. Fluid Mech.* **64**, 775–816.

BUSHELL, K. W. 1971 A survey of low velocity and coaxial jet noise with application to prediction. *J. Sound Vib.* **17**, 271–282.

CHAN, Y. Y. 1974*a* Spatial waves in turbulent jets. *Phys. Fluids* **17**, 46–53.

CHAN, Y. Y. 1974*b* Spatial waves in turbulent jets. Part II. *Phys. Fluids* **17**, 1667–1670.

CHAN, Y. Y. 1975 Non-linear spatial wave development in an axisymmetric turbulent jet. *NRL Aero. Rep.* no. 14756, LR 585.

CHAN, Y. Y. & TEMPLIN, J. T. 1975 Suppression of spatial waves by distortion of jet velocity profile. *Phys. Fluids* **17**, 2124–25.

CRIGHTON, D. G. 1975 Basic principles of aerodynamic noise generation. *Prog. Aerospace Sci.* **16**, 31–96.

CRIGHTON, D. G. & GASTER, M. 1976 Instability of slowly diverging jet flow. *J. Fluid Mech.* **77**, 397–413.

CROW, S. C. 1972 Acoustic gain of a turbulent jet. *Meeting Div. Fluid Dyn. Am. Phys. Soc. Univ. Colorado*, paper IEG.

CROW, S. C. & CHAMPAGNE, F. H. 1971 Orderly structure in jet turbulence. *J. Fluid Mech.* **48**, 547–91.

DAVIES, P. O. A. L., FISHER, M. J. & BARRATT, M. J. 1963 The characteristics of turbulence in the mixing region of a round jet. *J. Fluid Mech.* **15**, 337–367.

FISHER, M. J., LUSH, P. A. & HARPER-BOURNE, M. 1973 Jet noise. *J. Sound Vib.* **28**, 563–585.

FUCHS, H. U. 1972*a* Measurement of pressure fluctuations within subsonic turbulent jets. *J. Sound Vib.* **22**, 361–378.

FUCHS, H. U. 1972*b* Correlations of the fluctuating pressure in subsonic turbulent jets. *J. Sound Vib.* **23**, 72–99.

GRANT, A. J. 1974 A numerical model of instability in axisymmetric jets. *J. Fluid Mech.* **66**, 707–724.

GROSCHE, F. R. 1972 Investigation of the sound source distribution in turbulent gas flow. *Trans. DGLR Dtsche Gesellschafte für Luft- und Raumfahrt E. V., Berlin*, no. 6850.

HARDIN, J. C. 1973 Analysis of noise produced by an orderly structure of turbulent jets. *N.A.S.A. Tech. Note*, D 7242.

HOCH, R. G., DUPONCHEL, J. P., COCKING, B. J. & BRYCE, W. C. 1972 Studies of the influence of density on jet noise. *1st Int. Symp. Air Breathing Engines, Marseille.*

JONES, B. G. & PLANCHON, H. P. 1971 A study of the local pressure field in turbulent shear flow and its relation to aerodynamic noise generation. *N.A.S.A. Contractor Rep.* no. 134493.

KO, N. W. M. & DAVIES, P. O. A. L. 1971 The near field within the potential cone of subsonic cold jets. *J. Fluid Mech.* **50**, 49–78.

LAU, J. C. 1971 Ph.D. thesis, Southampton University.

LIGHTHILL, M. J. 1952 On sound generated aerodynamically. I. General theory. *Proc. Roy. Soc.* A **211**, 564–587.

LIGHTHILL, M. J. 1954 On sound generated aerodynamically. II. Turbulence as a sound source. *Proc. Roy. Soc.* A **222**, 1–32.

LIGHTHILL, M. J. 1961 Sound generated aerodynamically. Bakerian Lecture. *Proc. Roy. Soc.* A **267**, 147–182.

LIGHTHILL, M. J. 1963 Jet noise. *A.I.A.A. J.* **1**, 1587–1617.

LIU, C. H. & MAESTRELLO, L. 1975 Propagation of sound through a real jet flow field. *A.I.A.A. J.* **13**, 66–70.

LIU, J. T. C. 1974 Developing large-scale wavelike eddies and the near jet noise field. *J. Fluid Mech.* **62**, 437–464.

LUSH, P. A. 1971 Measurement of subsonic jet noise and comparison with theory. *J. Fluid Mech.* **46**, 477–500.

MCLAUGHLIN, D. K., MORRISON, G. L. & TROUTT, T. R. 1975 Experiments on the instability waves in a supersonic jet and their acoustic radiation. *J. Fluid Mech.* **69**, 73–95.

MATTINGLY, G. E. & CHANG, C. C. 1974 Unstable waves on an axisymmetric jet column. *J. Fluid Mech.* **65**, 541–560.

MICHALKE, A. 1971*a* Instabilität eines kompressibelen runden Freistrahls unter Berücksichtigung des Einflusses der Strahlgrenzschichtdicke. *Z. Flugwiss.* **19**, 319–328.

MICHALKE, A. 1971*b* New aspects of sound generation by circular jets. *Fluid Dynamic Trans.* **6**, 439–448.

MICHALKE, A. 1972 An expansion scheme for the noise from circular jets. *Z. Flugwiss.* **20**, 229–237.

MOORE, D. W. & SAFFMAN, P. G. 1975 The density of organized vortices in a turbulent mixing layer. *J. Fluid Mech.* **69**, 465–473.

MORFEY, C. L. 1970 Theory of sound generation in ducted compressible flows, with application to turbomachinery. Ph.D. thesis, University of Southampton.

MORRIS, P. J. 1971 The structure of turbulent shear flow. Ph.D. thesis, University of Southampton.

PETERSEN, R. A., KAPLAN, R. E. & LAUFER, J. 1974 Ordered structure and jet noise. *N.A.S.A. Contractor Rep.* no. 134733.

PFIZENMAIER, E. 1973 On the instability of a sound influenced free jet. *E.S.R.O. Tech. Trans.* no. 122. (Translation of *DFVLR Berlin Rep.* DLR-FB 73–69.)

SCHARTON, T. D. & WHITE, P. H. 1972 Simple pressure source model of jet noise. *J. Acoust. Soc. Am.* **52**, 399–412.

SCHUBERT, L. K. 1972 Numerical study of sound refraction by a jet flow. *J. Acoust. Soc. Am.* **51**, 439–462.

SMART, A. E. & MOORE, C. J. 1976 Aero engine applications of laser anemometry. *A.I.A.A. J.* **14**, 363–370.

VLASOV, YE. U. & GINEVSKIY, A. S. 1974 Generation and suppression of turbulence in an axisymmetric turbulent jet in the presence of an acoustic influence. *N.A.S.A. Tech. Trans.* F 15721.

WINANT, C. D. & BROWAND, F. K. 1974 Vortex pairing: the mechanism of turbulent mixing layer growth at moderate Reynolds numbers. *J. Fluid Mech.* **63**, 237–255.

WOOLDRIDGE, C. E., WOOTEN, D. C. & AMARO, A. J. 1971 The structure of jet turbulence producing noise. *N.A.S.A. Contractor Rep.* no. 126483.

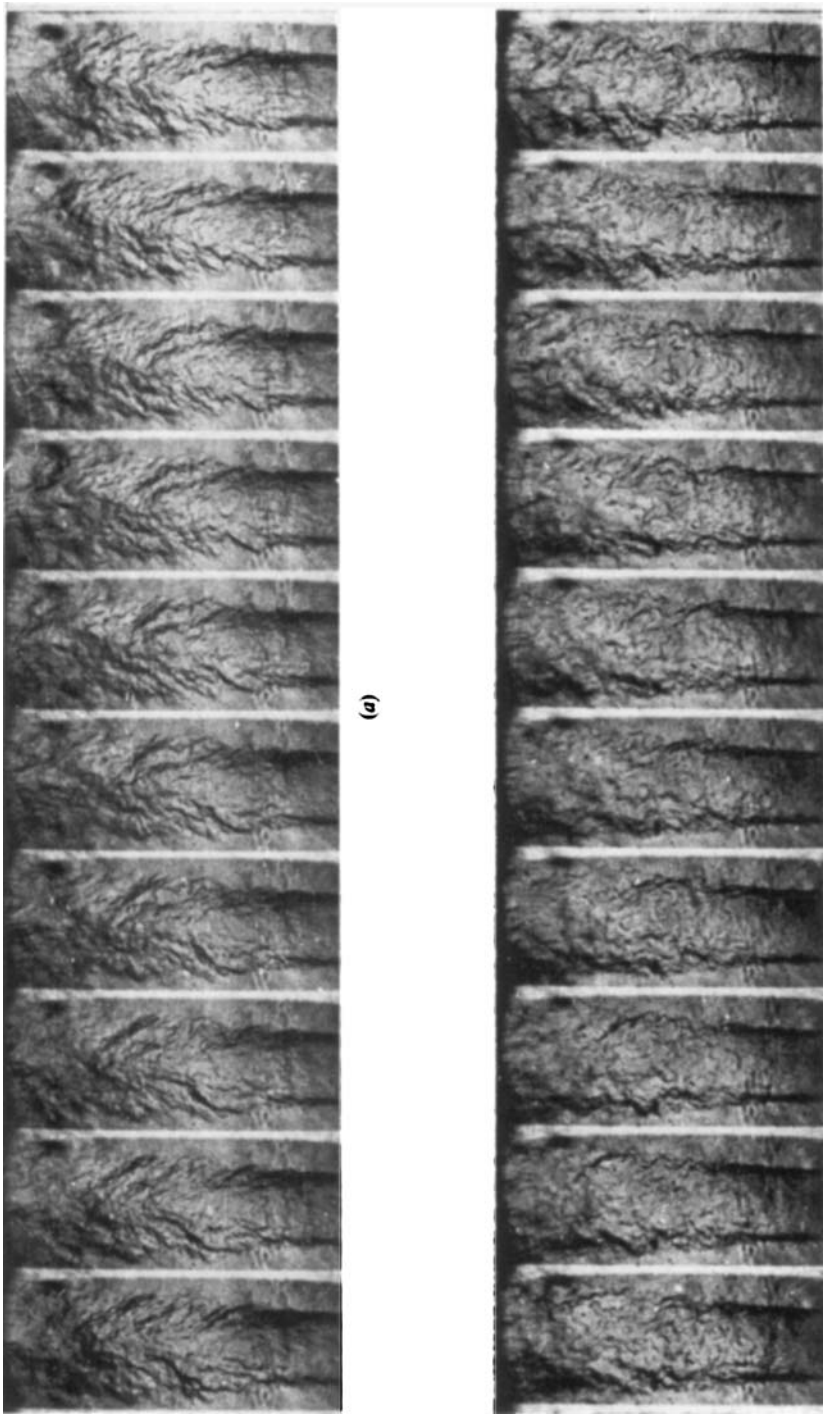

FIGURE 9. Some frames from a high-speed ciné schlieren film of the jet taken at 13500 frames/s. (*a*) $U_0/a_0 = 0{\cdot}3$, (*b*) $U_0/a_0 = 0{\cdot}83$.

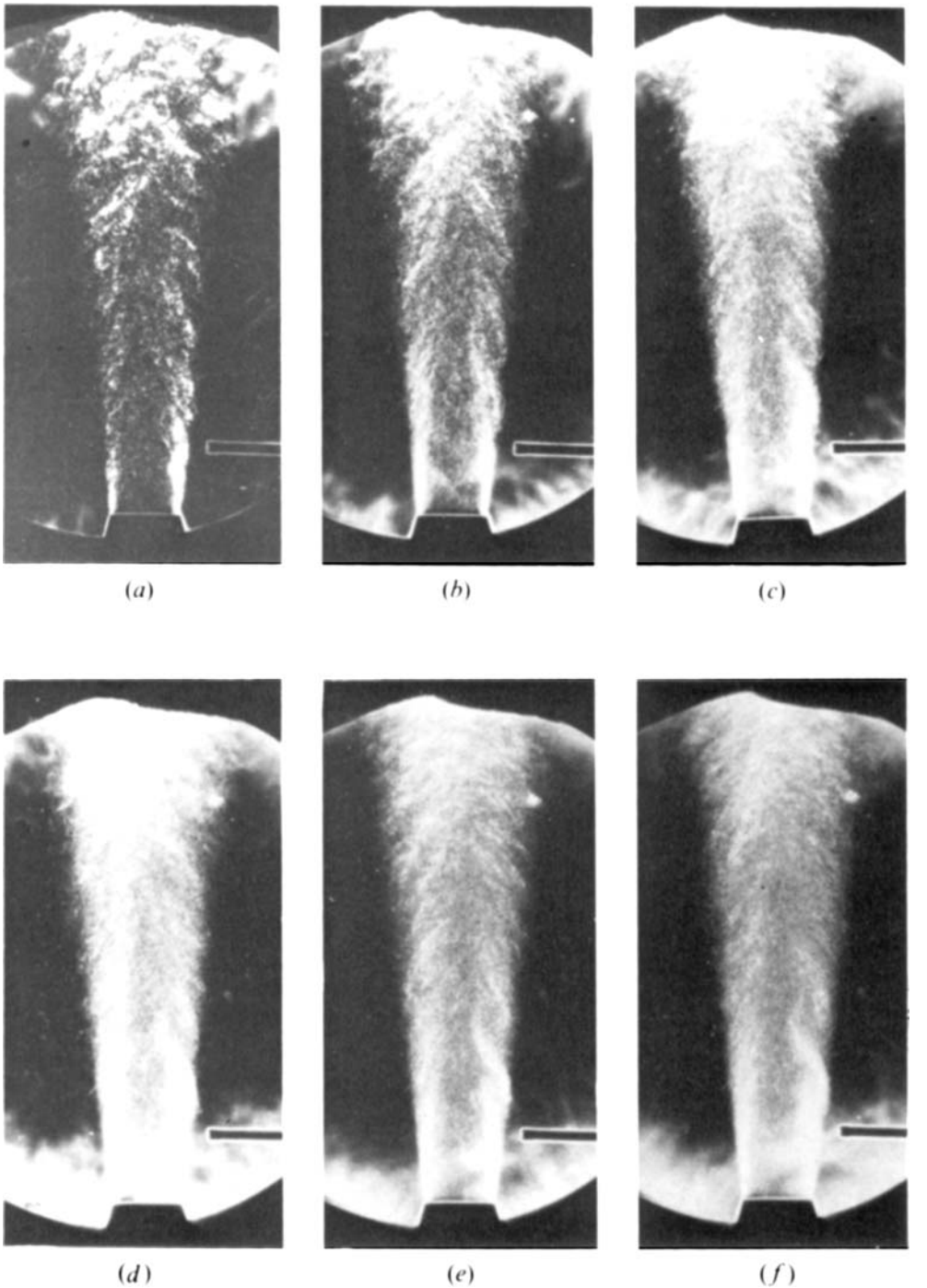

FIGURE 12. Demonstration of photographic averaging technique for different numbers of superimposed flashes: (*a*) 1, (*b*) 5, (*c*) 10, (*d*) 15, (*e*) 20, (*f*) 25.

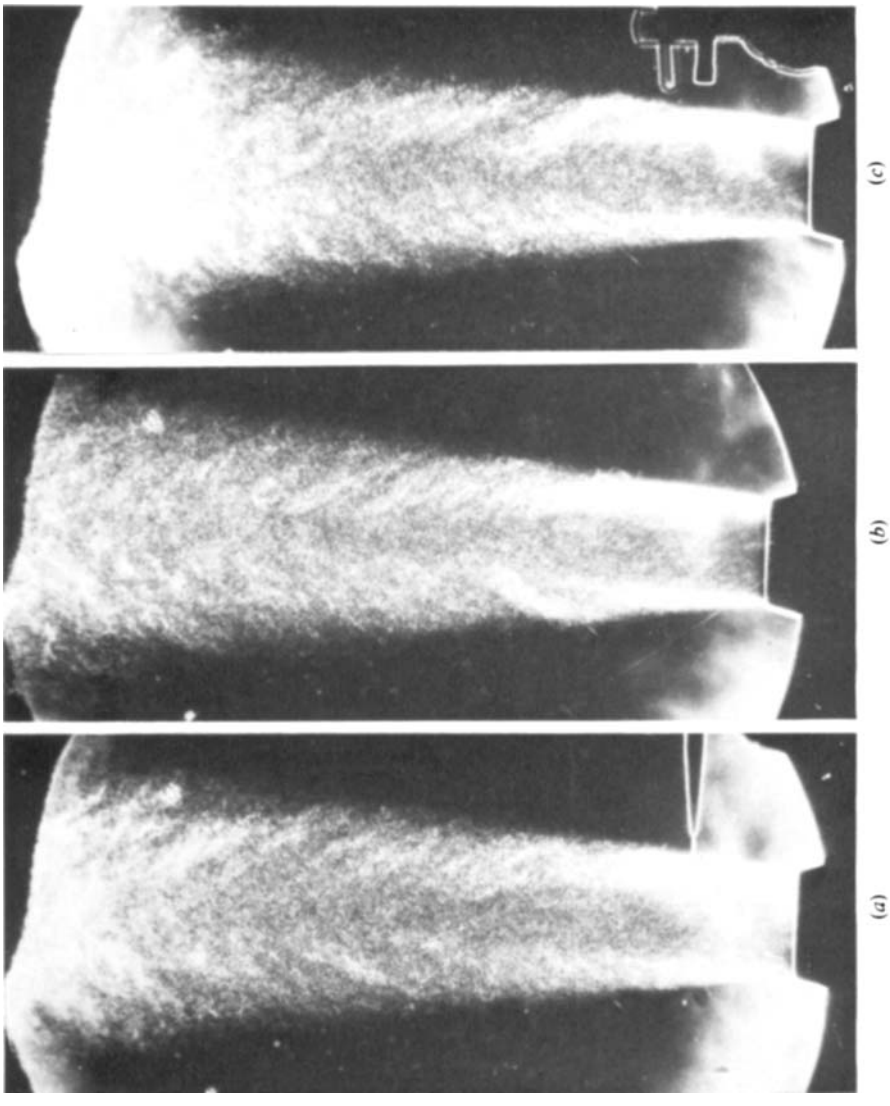

FIGURE 13. Averaging effect obtained using different trigger sources. (*a*) Hot-wire anemometer. (*b*) Laser-beam deflexion. (*c*) Microphone.

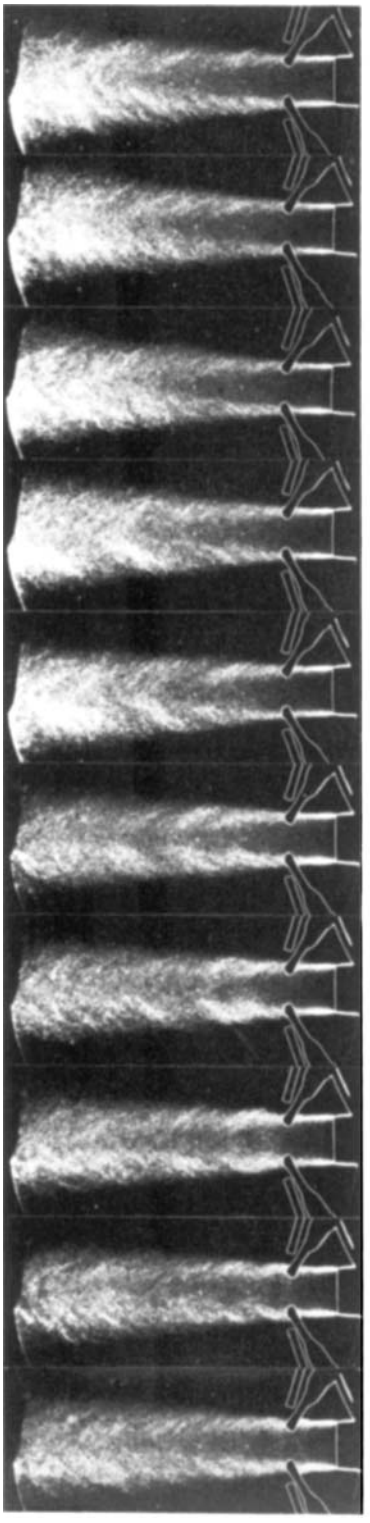

(*a*)

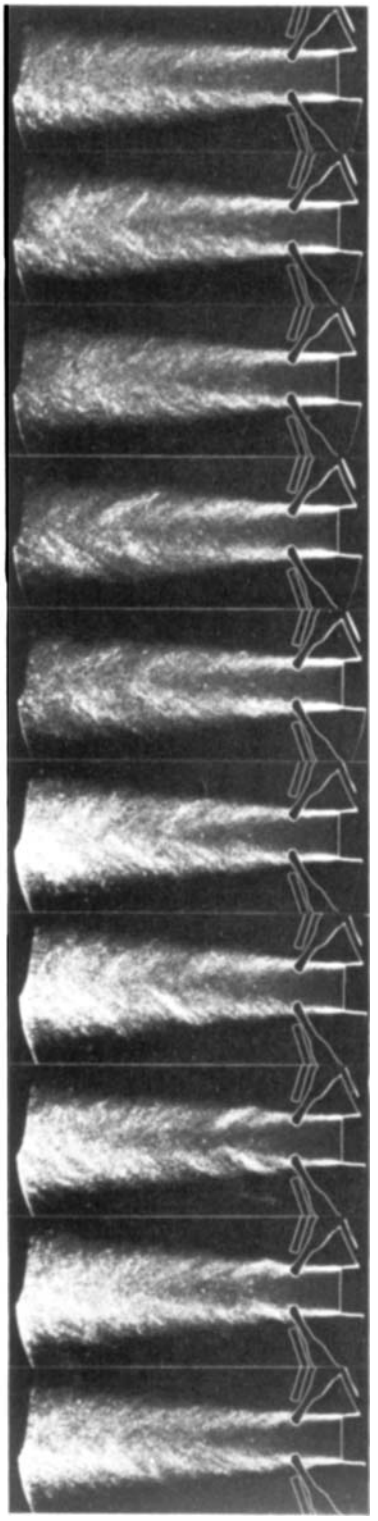

(*b*)

FIGURES 14 (*a*, *b*). For caption see plate 5.

(c) (d)

FIGURE 14. Multiple-exposure flash photographs of jet for increasing trigger delay. (*a*) $U_0/a_0 = 0{\cdot}3$, plane wave mode, (*b*) $U_0/a_0 = 0{\cdot}3$, first-order mode, (*c*) $U_0/a_0 = 0{\cdot}83$, plane wave mode, (*d*) $U_0/a_0 = 0{\cdot}83$, first-order mode. Delay between frames is 0·333 ms for $U_0/a_0 = 0{\cdot}3$ and 0·111 ms for $U_0/a_0 = 0{\cdot}83$. Last frame in each line is for random trigger.

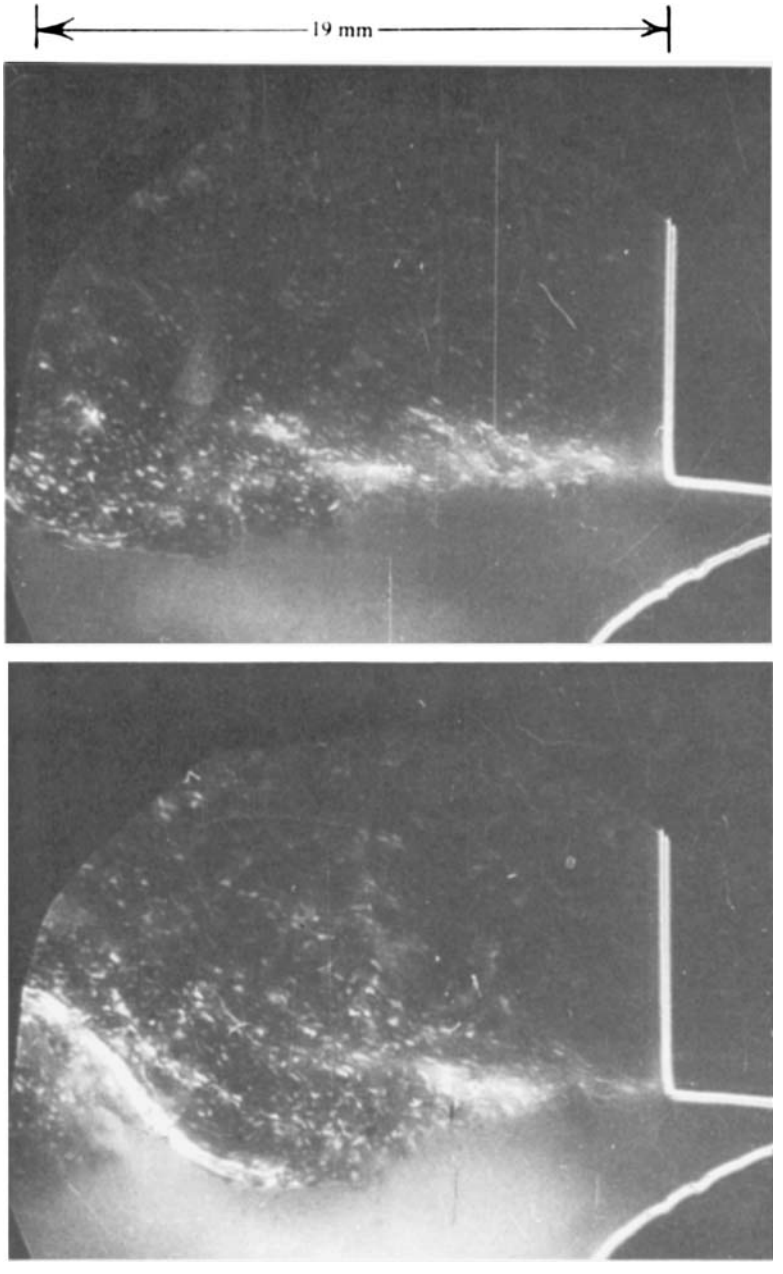

FIGURE 17. Single-exposure flash schlieren photographs of shear-layer disturbances near nozzle exit.

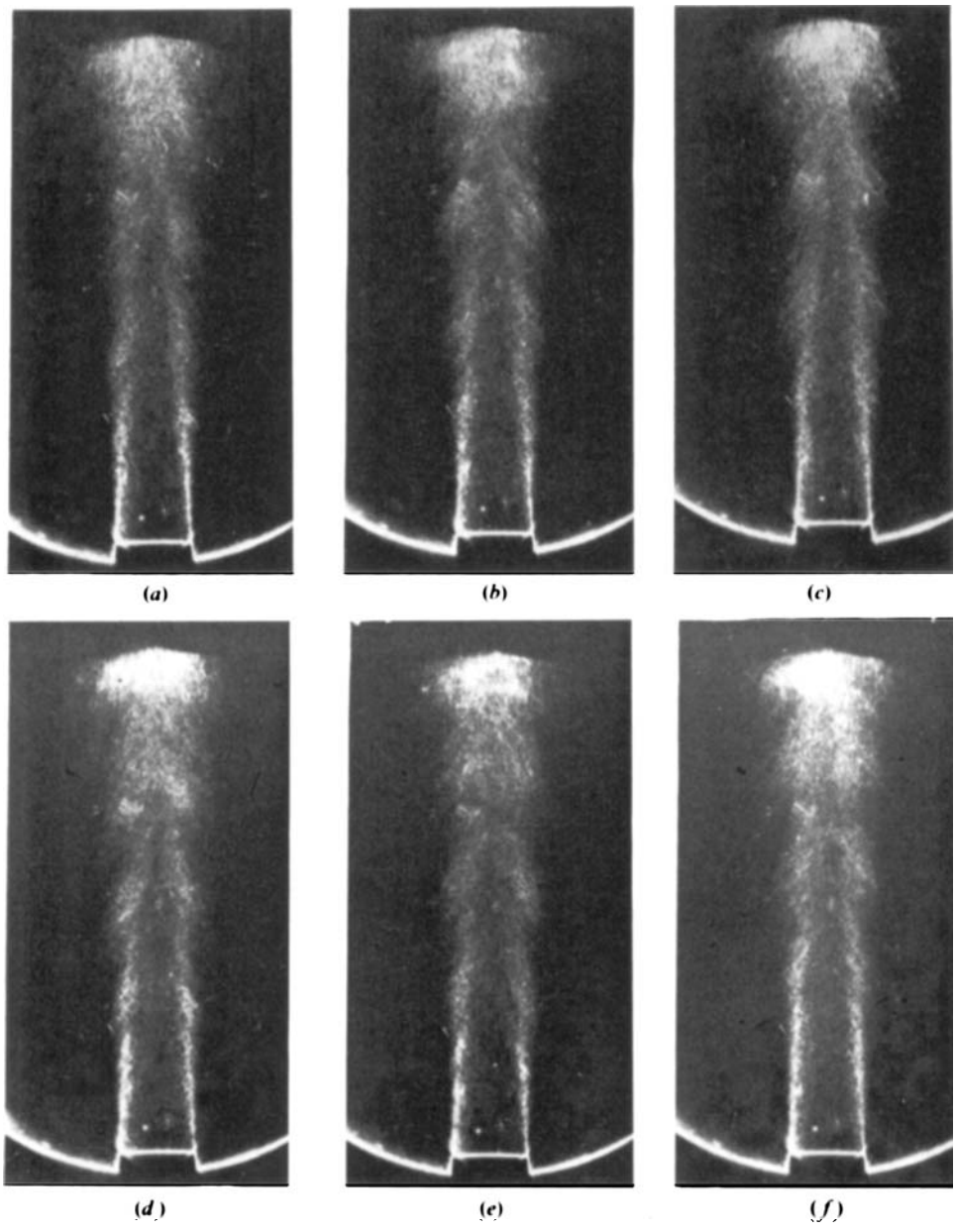

FIGURE 19. Multiple-flash schlieren photographs averaged with respect to an acoustic drive signal in the plenum chamber; $U_0/a_0 = 0{\cdot}49$, $f = 2$ kHz, relative delay. (*a*) 0 μs, (*b*) 88 μs, (*c*) 175 μs, (*d*) 263 μs, (*e*) 351 μs, (*f*) 438 μs.

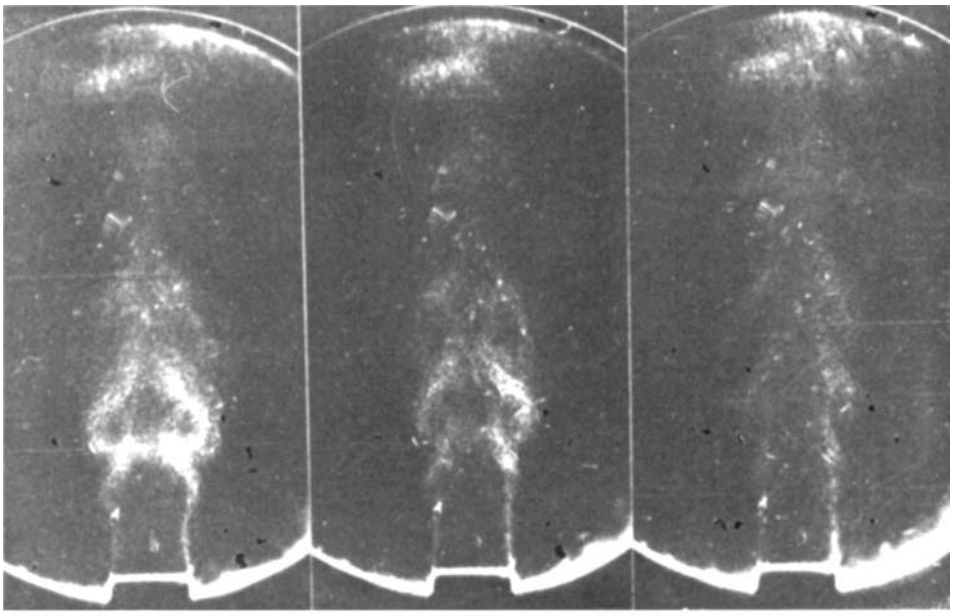

(i) (ii) (iii)

(*a*)

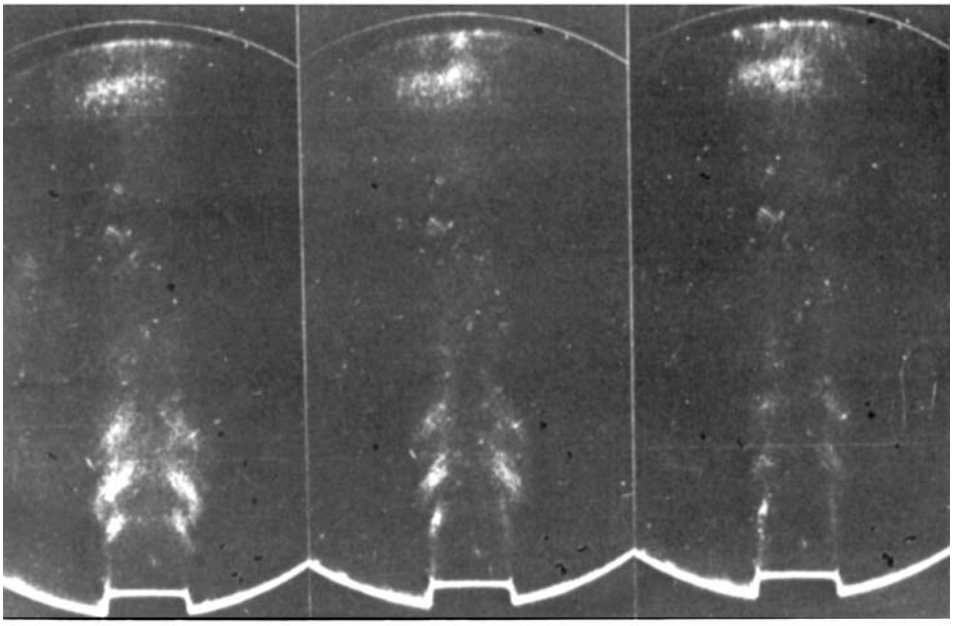

(i) (ii) (iii)

(*b*)

FIGURES 29 (*a*, *b*). For caption see plate 10.

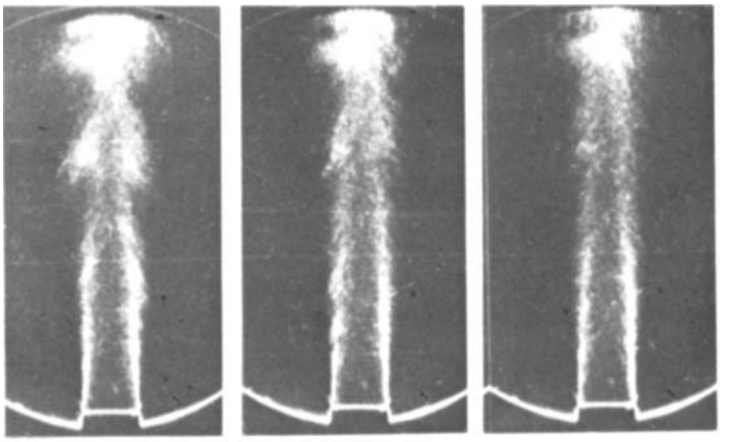

(i) (ii) (iii)

(*c*)

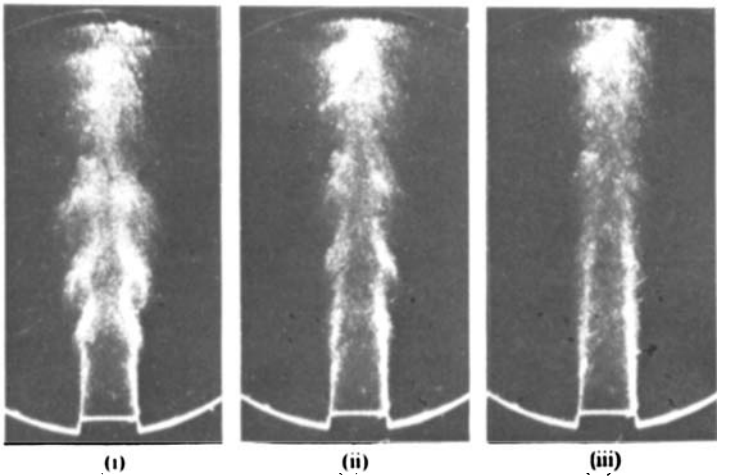

(i) (ii) (iii)

(*d*)

FIGURES 29 (*c*, *d*). For caption see plate 10.

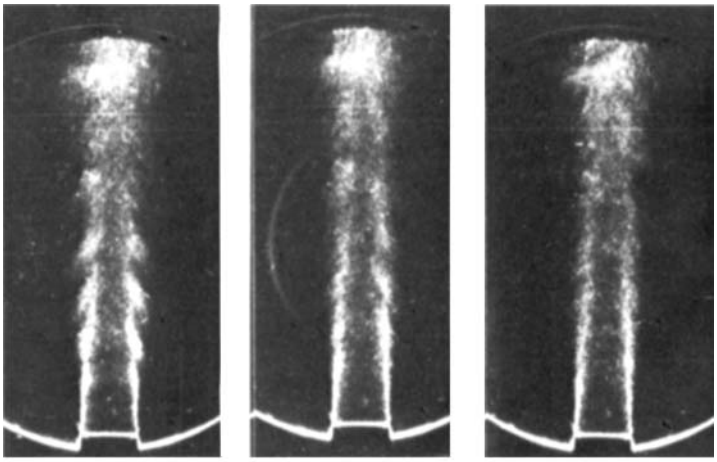

FIGURE 29. Effect of drive level on averaged schlieren photographs at jet velocities of (*a*), (*b*) $0{\cdot}3a_0$ and (*c*)–(*e*) $0{\cdot}49a_0$, and frequencies of (*a*), (*c*) 1281 Hz, (*b*), (*d*) 2050 Hz and (*e*) 3254 Hz. Frame (i) is for full drive; frames (ii) and (iii) are for reductions of 10 and 20 dB.